April 2018

Experimental Study of Flexible Electrohydrodynamic Conduction Pumping

Nathaniel J. O'Connor
Worcester Polytechnic Institute

Nicolas Vayas Tobar
Worcester Polytechnic Institute

Pavolas Nicholas Christidis
Worcester Polytechnic Institute

Experimental Study of Flexible Electrohydrodynamic Conduction Pumping

A Major Qualifying Project Report:
Submitted to the Faculty
of the
WORCESTER POLYTECHNIC INSTITUTE
in partial fulfillment of the requirements for the
Degree of Bachelor of Science
by

_____

Nicolas Vayas Tobar

_____

Pavolas Christidis

_____

Nathaniel O'Connor

April 25, 2018

Project Advisor:

_____

Professor Jamal S. Yagoobi, Advisor

Abstract

Electrohydrodynamics (EHD) deal with the interaction between electric fields and fluid flow. This interaction can result, for example, in electrically induced pumping, flow distribution control, or mixing of fluids. There are three kinds of EHD pumping mechanisms: ion-drag pumping, induction pumping, and conduction pumping. EHD pumps are advantageous for their small size and lack of moving parts.

This paper presents the design and performance characteristics of a flexible EHD conduction pumping technology in macro- and meso-scales. Specifically, the flow field generated by flexible EHD conduction pumps is measured on a flat-plane and in various internal and external configurations. The results show that the flexible EHD conduction pumps are readily capable of generating significant flow rates in macro- and meso-scales by simply inserting them into the desired setups. Unlike mechanical pumps, flexible EHD conduction pumps are lightweight, can flex into complex geometries such as a cylinder or cone. Additionally EHD conduction pumps can be scaled down to the micro-scale which is impossible for a mechanical pump. This technology shows potential for use in a wide range of applications, including thermal control of flexible electronics, cooling of high power electrical systems, actuators for soft robotics, and medical devices.

Acknowledgements

First, we would like to thank Worcester Polytechnic Institute and the Mechanical Engineering Department at WPI for the providing the necessary resources to complete this project. We would like to thank our advisor, Professor Jamal Yagoobi for providing guidance during the project. We would also like to thank Michal Talmor, a PhD candidate at WPI, for the help with designing, assembling and running the experimental setup described in this report. Their guidance was essential to the development of this project. We would like to acknowledge the professional vendors we have had the pleasure to work with: TechPrint Inc. Lastly, we would like to recognize the NASA Headquarters Fluid Physics Program which partially funded the project.

Table of Contents

Table of Figures

Table of Tables

Chapter 1: Introduction

Overview of Electrohydrodynamics

Electrohydrodynamics (EHD) studies the interaction between electric fields and fluid flow. EHD pumping, the process of pumping dielectric fluids by injecting ions into them, has been a known phenomenon for over a century, but rigorous study of it only began in 1959 (Stuetzer, 1959, Pickard, 1963, Melcher, 1961). There are currently three different types of EHD pumping, the most reliable of these being EHD conduction pumping. EHD conduction pumping has been primarily used to enhance the heat transfer capabilities of cooling systems in aerospace applications. It is currently being tested on the International Space Station, with an additional experiment scheduled for 2021.

The underlying physics behind EHD pumping identifies three main forces involved in the interactions between the applied electric field and the working fluid. The process was described theoretically by coupling the Navier-Stokes equations to the Maxwell equations (Atten and Seyed-Yagoobi, 1999). This is seen through the electric body force equation which describes the electrical fields and flow fields interaction:

$$\bar{f}_{EHD} = \rho_e \bar{E} - \frac{1}{2} E^2 \nabla \varepsilon + \frac{1}{2} \nabla \left[E^2 \rho \left(\frac{\partial E}{\partial \rho} \right)_T \right] \quad (1)$$

In the above equation, $\bar{f}_{EHD}$ is the total body force on the working fluid due to an applied electric field. ρ_e represents the charge density, E represents the electric field strength, and E is the permittivity of the working fluid. ρ is the mass density of the working fluid and $\frac{\partial E}{\partial \rho}$ is determined at a constant temperature. The first term represents the Coulomb force that acts on free charges in an electric field and is the dominant force in EHD pumping. The second and third terms are the dielectrophoretic and electrostriction forces respectively, which represents the

polarization force acting on polarized charges. The dielectrophoretic force is dependent on a gradient in permittivity which does not exist in an isothermal liquid. The electrostriction term requires permittivity to be a function of the density of the fluid at a constant temperature. For the case of incompressible fluids, this term is negligible. Therefore, the force on the free charges in the fluid is majorly dependent on the electric field vector.

To incorporate the effects of the EHD phenomena in the mechanics of the fluid, the Navier-Stokes equations must be analyzed. The Navier-Stokes equations relate the characteristics of a fluid to its velocity, pressure and energy. The first equation on the set, is the continuity equation, related to the conservation of mass on the fluid domain. The second equation describes the forces present in the fluid. On the left-hand-side of the second equation, the term represents the flow inertia. On the right-hand-side the terms represent the surface force, the viscous shear-stress force, the body force, and the electric body force, when read from left to right. The third equation, known as the energy or energy conservation equation, describes the total energy of the system. In the EHD case this last equation has the Joule heating term included, which describes the relationship between the electrical conductivity of the fluid and the applied electric field. In this way, EHD contributes both to the flow and the total energy of the fluid.

$$\nabla \cdot \bar{u} = 0$$

$$\rho\,(\bar{u}\cdot\nabla)\,\bar{u} = -\nabla P + \mu\,\nabla^2\,\bar{u} + \rho\,\bar{g} + \bar{f}_{EHD}$$

$$\rho\,c_p\,(\bar{u}\cdot\nabla T) = k_l\,\nabla^2\,T + J_e$$

There are three EHD pumping mechanisms based on the Coulomb force: conduction pumping, induction pumping, and ion-drag pumping. These methods differ from one another by the way they generate a non-zero net charge density which allows the Coulomb force to have an effect. EHD conduction pumping has shown extensive potential due to simple non-mechanical design, low power consumption, low acoustical noise generation, low weight, and ease of pumping control by adjusting applied voltage.

Project Overview

The goal of this project is to take already proven EHD conduction pumping technology and apply it to flexible materials. These flexible EHD conduction pumps are the first non-mechanical flexible pumps ever created. Flexible EHD conduction pumps would retain all the advantages of rigid EHD conduction pumps while having improved capabilities and characteristics. To mention a few, they are adaptable, lightweight, inexpensive and easy to manufacture. The choice of material greatly reduces the weight compared to the rigid counterparts. The material also offers the advantage of being able to bend and change shape as needed, allowing them to be placed in unique and complex geometries. As much as the efficiency decreases from the rigid to these flexible pumps, performance and reliability are still comparable to previously studied rigid pumps. Furthermore, these pumps are highly useful for the changing needs of the industry: the simple design and manufacturing offer scalable pumps that can adapt to various geometries.

EHD Pumping Mechanisms

As mentioned earlier, there are three EHD pumping mechanisms that have been explored over the years: conduction pumping, induction pumping, and ion-drag pumping (Seyed-Yagoobi,

2005). Each of these mechanisms generates flow by imposing electric fields which affect charges in dielectric fluids. Dielectric fluids have very low electrical conductivity and do not have a net charge innately. Each mechanism introduces free charges into the dielectric fluid in a different manner. Because the pumping mechanism utilized in this Major Qualifying Project is conduction pumping, this mechanism will be described in depth, while the other two will be discussed briefly.

Ion-Drag Pumping

Ion-drag pumping requires direct injection of free charges into a dielectric working fluid. This is accomplished using a sharp corona source, known as an emitter electrode, to inject ions. These ions are collected by an oppositely charged electrode, known as a collector electrode. The flow of the injected ions between the emitter and collector causes a net flow of the working fluid to occur. This type of EHD pumping was the first pumping mechanism to be explored and is therefore well documented. However, this pumping mechanism has a significant disadvantage which makes it unsuitable to commercial use. The ion injection from the emitter electrode causes the electrode to deteriorate as its material is injected into the fluid. The additional charges injected into the working fluid also deteriorate the electrical properties of the dielectric working fluid, causing performance to degrade and eventually fail. Although this EHD pumping mechanism is capable of relatively high pressure generation, its applications are severely limited for any device which requires continuous operation. (Seyed-Yagoobi, 2005).

Induction Pumping

Induction pumping is an EHD pumping mechanism that uses an electric AC traveling wave to attract or repel induced charges in the dielectric working fluid. The dielectric fluid does not normally have a net charge, but charges can be induced in the fluid by a discontinuity of the electrical conductivity of the fluid, either by an imposed thermal gradient or change of phase. Therefore, this EHD pumping mechanism is primarily used where phase changes or significant temperature differences are present. Different flow velocities can be generated in the working fluid by changing the frequency and voltage of the traveling wave. This pumping mechanism was originally explored in the 1990's and has since been explored as a method of pumping thin fluid films and liquid/vapor phases. However, this pumping mechanism cannot be used for isothermal applications (Seyed-Yagoobi, 2005).

Conduction Pumping

Conduction pumping uses the dissociation of naturally occurring electrolytic impurities within a dielectric working fluid as a source of free charges. A neutral species, AB, and its positive and negative ions, A+ and B-, constantly dissociate and recombine in the dielectric fluid.

$$AB \underset{\text{Recombination}}{\overset{\text{Disocciation}}{\longleftrightarrow}} A^{+} + B^{-}$$

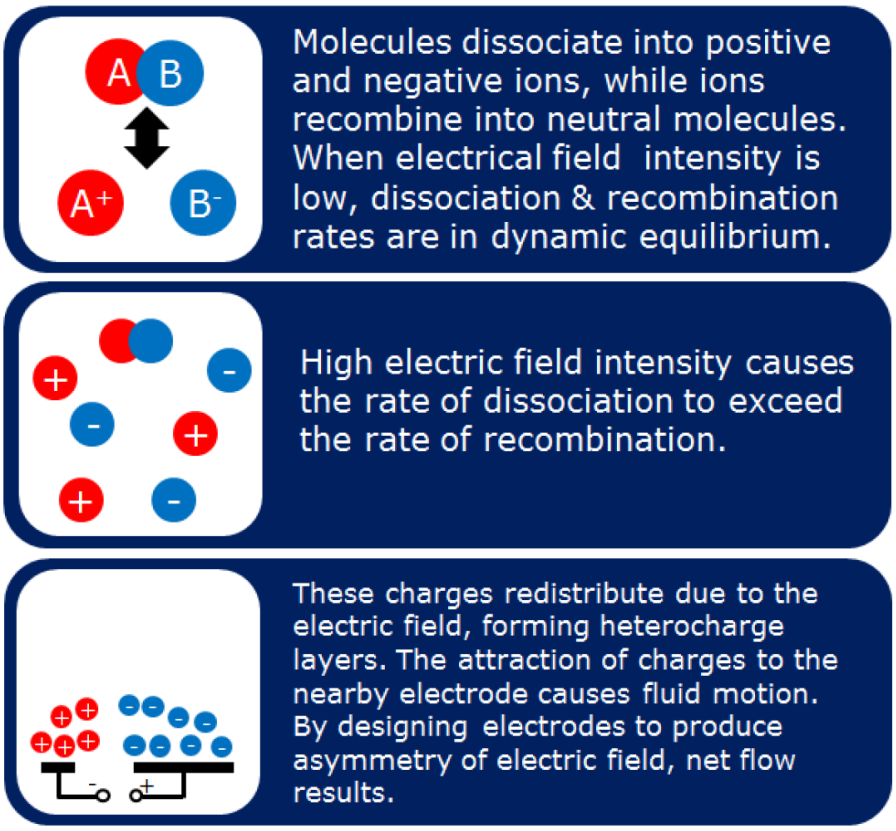

Figure 1: Description of the EHD phenomenon to a moleculear level.

When the imposed electric field exceeds a threshold, typically on the order of 1kV/cm depending on the fluid characteristics, the rate of dissociation exceeds the rate of recombination. Ion motion is caused by the Coulomb force described above and results in a non-equilibrium layer of charge in the vicinity of the electrodes, known as the heterocharge layer. The thickness of the heterocharge layer depends on the dielectric fluid properties and the applied electric field. The attraction of the heterocharges to the adjacent electrodes causes a bulk fluid motion. Changing the applied potential immediately changes the generated flow. A schematic depicting the heterocharge layers with fluid flow direction is shown in Figure 2 (Patel and Seyed-Yagoobi, 2014).

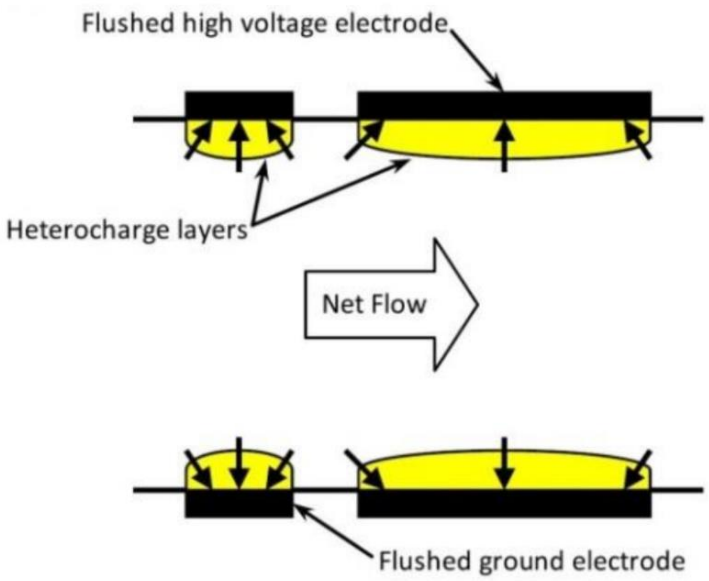

Figure 2: Heterocharge layer formation around flush electrodes.

In this pumping mechanism it is not required to generate a discontinuity in the conductivity of the dielectric fluid. Therefore the working fluid can be regarded as isothermal and incompressible, and the net body force equation can be reduced to the following:

$$\bar{f}_{EHD} = \rho_e \bar{E} \qquad (2)$$

The electrodes are required to be asymmetric in shape in order for a net body force to be generated, If the electrodes are symmetric, the negative and positive charge densities cancel out and no net body force is generated and no flow is generated.

This pumping mechanism has been preferred over the two earlier ones due to its reliable long term operation and simple electrode design (Jeong et al, 2003). This pumping mechanism is very reliable because no additional heat needs to be applied to the working fluid and there is no degradation of the working fluid from additional ion injection. While this pumping mechanism requires relatively high input voltages, the current consumption is extremely low, and thus the power consumption is very low. Various designs have been proposed to use EHD conduction pumping in open channel and enclosed configurations, proving to be independently successful

(see Atten and Seyed Yagoobi 1999; Hanaoka et al 2004; Jeong and Seyed-Yagoobi 2004; Patel 2011; Pearson and Seyed-Yagoobi, 2013; Louste et al, 2005).

Overview of Flexible Electronics

Flexible electronic started in the 1960s with the development of thin solar cells (Wong, 2009). The reduced thickness of cells made them bendable, elastic, and lightweight. Soon after, thin-film transistors started using thin substrates like polyethylene and Mylar. Similarly, the great reduction in size of electric circuits, led to small scale electronics that were on the limit of rigidity. By 1990, the Japanese LCD industry started using chemical vapor deposition (CVD) and photolithography in these substrates. Progressively, a variety of industries, from the medical industry to the arts, started adopting flexible electronics as part of components and big systems. Currently, flexible electronics are a solution for adaptable electronics that need to be within non-rigid systems.

According to Wong and Salleo, flexible electronics are composed of "(1) a substrate, (2) backplane electronics, (3) a frontplane, and (4) encapsulation" (2009). For the system to work appropriately, all these components need to maintain functionality while being flexed. The substrate, generally a highly resistive polymer, acts as a canvas for the electronics. The encapsulation can be seen as a coating on the electronic component or as a separate component to protect the electronics. These four components can be seen in circuits, displays, actuators, and sensors. In this way, an in-depth consideration of the materials that come to make these components is needed to make flexible electronics.

Flexible electronics have many potential applications, with some analysts predicting that the printed electronics market will eventually be comparable to conventional silicon electronics (Chang, 2012). It is expected that the market for printed electronics will grow to US$44.2 billion

in 2021. Printed electronics also tend to be much faster to produce with additive processes rather than traditional subtractive processes. The traditional subtractive processes include photolithography and laser ablation. Some additive processes include screen printing, inkjet, and flexographic. These additive processes general have a lower resolution of 10-50μm compared to subtractive processes with a resolution lower than 10μm. However, the additive processes have a significant advantage in throughput and production time. These additive methods allow for large scale roll to roll printing similar to large scale paper printing. The processes are generally more 'green' in that they use less harsh chemicals in production. Possibly more important for the industry than the previously mentioned advantages, the additive processes for creating flexible electronics is also cheaper than traditional subtractive methods (Chang, 2012).

Flexible electronics, while often being regarded as an important evolutionary step in development of electronic products, are not without challenges (Bedell et al, 2014). The largest limitation of flexible electronics is that its performance is lower compared to a traditional rigid system due to the materials used having a lower charge carrier mobility (Wu, Huang, & Chen, 2017). Because of this disadvantage, flexible electronics will need to be implemented into particular applications, such as novel medical devices or actuators for soft robotics. Flexible electronics on soft actuators could be used for heart treatments or timed drug release. While there are many novel applications for flexible electronics, it will take years for the technology to mature enough to become standard in industry.

As discussed previously, EHD conduction pumping happens as a result of the interaction between the electric fields and fluid flow fields. To a component level, this interaction is seen between the electrodes and the dielectric fluid medium. Having front plane electronics as the electrodes, allow for this interaction to happen. However, the front plane electronics need to

withstand the high-voltages used in EHD conduction pumping, the fluid interactions, and the prolonged use. This paper follows a design process that considers these requirements of EHD conduction pumping and finds suitable materials to adapt rigid EHD pumps to flexible EHD pumps.

Potential Applications

As previously mentioned, EHD conduction pumping offers advantages over other pumping mechanisms such as simplicity of design, reliability, and scalability to the micro-scale. These pumps have the most immediate and obvious applications in space. These pumps can be implemented into cooling systems in both spacecraft and satellites due to their reliability and low weight. These pumps are also able to function effectively in microgravity with systems that require low differential pressure to move fluids. The ability to more efficiently remove heat from electrical components on satellites has significant advantages, as this is one of the current limitations on today's satellites. Previous EHD conduction pumping studies have shown up to significantly increase critical heat flux in pool boiling systems (Pearson & Seyed-Yagoobi, 2013) . With this technology, more powerful processors can be integrated into satellites, which in turn can improve weather forecasts, GPS accuracy, or defense of the nation.

EHD conduction pumping has been experimented with as a method for smart flow control in recent years (Feng & Seyed-Yagoobi, 2006). In many cases of parallel flow heat exchangers, not all lines receive the same flow rate which results in inefficiencies. Positioning EHD conduction pumps at the inlets would allow smart control of the flow rate of each parallel tube. EHD conduction pumps are easily controlled with applied voltage and have a near instant response time, so a system could automatically adjust the voltages to evenly distribute flow through the heat exchanger.

Another application on the horizon for EHD conduction pumping is implementation into the vapor compression cycle. EHD conduction pumps would be embedded into the evaporator to enhance heat transfer and increase the temperature of the working fluid going to the compressor. This would reduce the inlet pressure of the compressor and eliminate the pressure drop. Additionally, the load on the compressor could be reduced to make it a smart compression cycle capable of adjusting the condensation rate of humid air. WPI's Multiscale Heat Transfer Laboratory will be exploring this concept over the next few years. The ultimate goal is to improve the coefficient of performance of the compressor from its current average of about 4, up to about 6. Increasing this coefficient of performance, or the ratio of heat supplied or removed from the system to the work required by the system, would greatly reduce power consumption across the country. This more efficient vapor compression cycle will also be explored as a method from producing pure water from air for those who need it around the world.

Chapter 2: Methodology and Experiment Design

Overview

The goal of this Major Qualifying Project was to apply EHD conduction pumping to flexible materials and create a flow field in different configurations of the pump. The pumps were designed in macro and meso-scales as determined by their electrode size and spacing. There were five additional design objectives for this device and the experiment in addition to serving as a proof of concept:

- The pump must operate without degrading in the dielectric corn oil
- The pumps must be able to operate under the required voltages to produce flow
- The pumps design must be simple and able to be replicated for future designs
- The pumps can be easily prototyped, manufactured, and reproduced
- The fluid velocity along the electrodes must be measured

First we considered many different materials which could be used to fabricate these pumps. The substrate material needed to be made of a polymer material, as they are both flexible and insulating. The electrodes needed to be very conductive, while also being able to easily flex without plastic deformation. These electrodes would be made of a metallic material, and thus would need to be extremely thin, even relative to the substrate.

After material properties were considered, we fabricated an initial prototype using copper conductive tape with a PET film. This initial prototype allowed us to verify our design would be feasible using thin film materials. The initial prototype had flaws such as sharp edges and dimensional accuracy which were considered and remedied in the second iteration of the design. The fabrication of the pumps was outsourced to a local company that specialized in printed electrical circuits. We created five different pump designs which were screen printed using a

conductive silver ink on a PET substrate. These five pumps are those which were tested and appear in the results.

The pumps were tested in an open tub system connected to a high voltage power supply. A LabVIEW program remotely controlled the voltage and measure current across the pump. Velocity data was measured using PTFE particles recorded from a top view by a camera. While these pumps produced good results, they were not without issues of their own, which were remedied in a set of final designs which are found in the discussion section of this project report.

Material Selection

As previously mentioned, flexible electronics have four components, all of which need to have appropriate material selection for their use in the required application, in this case EHD conduction pumping. This pumping mechanism has specific requirements: a dielectric fluid medium, highly conductive electrodes, ability to withstand high voltages, and reliable over long periods of time. These requirements, together with our design objectives, determined the type of materials we used.

For the conductive material, we examined five different metals. For each metal we analyzed its properties in relation to the environment it is exposed to and to flexibility. Since electricity was being run through the electrodes, the electrode material needed to be highly electrically conductive. One constraint for selecting the materials for the electrode was whether or not the corn oil would corrode the pump. Another constraint was its material properties to be used in a flexible system, such as the Young's Modulus. Using CES EduPack 2017 to research properties of materials, five metals were tabulated and compared certain properties. With the known Young's Modulus and the distance covered to flex the pump into a half-cylinder, the

maximum thickness to avoid plastic deformation was calculated for each metal. These properties and the maximum thickness is shown in the table below:

Table 1: Properties of metals considered to be used as the electrode material.

Electrode Material	Conductivity (10^7 S/m)	Conductivity	Durability in Veg. Oil	Tensile Strength (MPa)	Young' Modulus (GPa)	Thickness (mm)
Copper	2.00 - 5.75	Good	Good	100 - 400	112 - 148	<0.0625
Nickel	1.00 - 1.25	Good	Good	345 - 1000	190 - 220	<0.0789
Cast Al	2.00 - 4.00	Good	Good	65 - 386	72 - 89	<0.0694
Brass	1.00 - 1.25	Good	Good	310 - 550	90 - 110	<0.1056
Silver	5.52 - 5.99	Good	Fair	255 - 340	69 - 73	<0.0797

Various polymers like PTFE, PFA, PE, PET, and rubber were considered for the substrate material. Similar to the electrode material, we had to consider corrosion in oil. However, in this case the material needed a high resistivity to avoid electrical conduction. Rubber is soft and malleable, which we wanted for our application. However, its porosity would soak the vegetable oil. Plastics such as PTFE and PFA, do not retain their original shape when bent or rolled which is not ideal for a flexible pump. For this, we mainly focused on PET as it is the substrate used most extensively in flexible electronics, and had the desired properties for our application. PET can also be transparent which was essential to our decision. The table below shows a few of the properties we considered for the evaluation of the materials.

Table 2: Properties of polymers considered to be used as the substrate material.

Substrate Material	Resistivity (10^21 Ohm.m)	Resistivity	Resistance to Veg. Oil	Tensile Strength (MPa)	Young's Modulus (GPa)	Dielectric Constant
PTFE	330 - 3000	Good	Good	20.7 - 34.5	0.4 - 0.552	20 - 2.2
PET	0.33 - 3.00	Good	Excellent	48.3 - 72.4	2.76 - 4.14	3.5 - 3.7
PEN	7.14 - 14.00	Good	Good	46.4 - 48.8	2.37 - 2.43	2.9 - 3.2
PFA	300 - 3000	Good	Good	27.6 - 29.6	0.47- 0.49	2 - 2.2
PDMS	0.25	Good	Good	1.79 - 2.24	0.2	2.3 - 2.8
Si Rubber	0.03 - 10.00	Good	Fair	2.4 - 5.5	0.01 - 0.02	2.9 - 4.0

Based on these properties, we needed to decide on a manufacturing process that would adhere the electrodes to the substrate. A few methods were considered: chemical and electron vapor deposition, metal etching from a substrate coated in metal, screen-printing, and conductive tape adhered to the substrate. The availability of all the methods was examined, determining that vapor deposition was both limited on campus and on prototyping manufactures for scales greater than 1 cm^2. Etching requires some hard chemicals that we could not access to remove the conductive layer in a specific geometry from a plastic and conductive material film. This led us to have just two accessible manufacturing mechanism, conductive tape over the substrate and screen-printing, which will be compatible with the required properties established previously.

Copper Tape Prototype

The first design of the flexible EHD conduction pump had the goal of proving that EHD conduction phenomenon could be applied to flexible materials, as a flexible EHD conduction pump has never been developed before. This initial pump was designed in what is known as the "macro-scale" because it was being fabricated by hand. In EHD conduction pumping

terminology, the scale of the pump is based on the size of its electrodes and their spacing and a property known as the “characteristic length”. The characteristic length is defined as the spacing of between the ground an high voltage electrodes, and all other dimensions of the pump are a ratio of this characteristic length. Macro-scale pumps possess a characteristic length of greater than 1mm. Meso-scale pumps have a characteristic length between 250 um and 1 mm. Micro-scale pumps have a characteristic length below 250 um. The characteristic length and other dimensions of this initial prototype are provided in detail below. The first pump was designed on a flat plane so it could be flexed into different shapes such as a tube or half cylinder along multiple directions. It was designed similarly to previous rigid EHD conduction pumps such as those created by Siddiqui and Seyed-Yagoobi in 2009.

The macro-scale pump differed in a few ways from the pump created by Siddiqui and Seyed-Yagoobi. First, the buslines used to connect all of the ground electrodes together and high-voltage electrodes together were placed on the same side as the electrodes. This simplified the design of the pump because through holes were not necessary to connect the buslines in the backplane of the substrate to the electrodes in the front plane. It also made the pump easier to manufacture as the electrodes were adhered to the substrate by hand using an adhesive. Additionally, solder plates were added and are located at the end of the buslines. The solder plates allowed for easy connection to the high-voltage power supply. Wires could be soldered directly to the plates or some other connector could be attached to them.

Finally, the electrode sizing and spacing ratios for optimal pump performance were numerically determined by Siddiqui and Yagoobi in 2009. The ground electrode and spacing between the ground and high voltage electrode have a ratio of 1:1 ratio and are both equal to the characteristic length. The size of the high voltage electrode was 3 times the characteristic length,

while the spacing between electrode pairs has a 2:5 ratio compared to the characteristic length. With regard to the first design of the macro-scale pump, the ground electrode and characteristic length was 2.12mm. Therefore, the high-voltage electrode is 6.36mm and the electrode pair spacing is 5.30mm, consistent with the optimal ratios mentions. In total, ten electrode pairs were placed on the pump and the total pump size was 78.24mm x 185mm. Increasing the number of electrode pairs increases the generated flow almost linearly. Figure 3 shows the optimal electrode size and spacing used in all of the pumps designed.

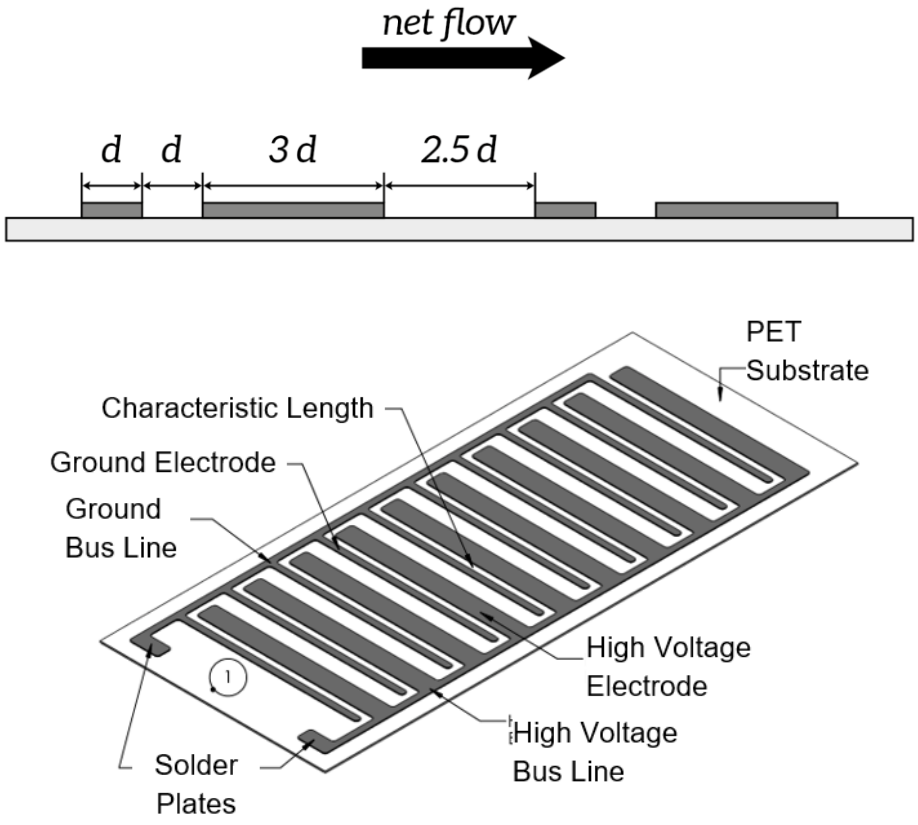

Figure 3: (a) Optimal electrode size and spacing, (b) diagram of EHD conduction pump

The macro-scale pump was created using the copper tape and PET film. The copper tape was highly conductive, incorporated a conductive adhesive, and was capable of adhere to solder. It also had a thickness of 0.0889 mm which is not less than the thickness found in Table 1,

however it was the only thin metal with adhesive found at a reasonable cost. The PET film found was a sheet that was 0.762mm and was also transparent.

For this design, we needed to minimize the sharp edges present on the electrodes to prevent charge injection while maintaining the necessary precision for the design. To achieve this, four processes were considered to cut the electrodes out of the copper tape. First, machine cutting was evaluated, finding that the common methods to cut metal sheets included laser cutting, water jet cutting, and vinyl cutting. A laser-cutter would be the most effective and precise way to cut the copper tape. However, there were no laser-cutters at WPI that could cut through metal, no matter the thickness. Laser cutters in machining shops in Worcester, like Technocopia, could cut metal only with thickness greater than ¼ in. Similarly, the vinyl cutter was found to be too weak to cut the metal, and the water-jet too powerful, potentially ruining the tape. Second, a cookie-cutter-type part could achieve cutting precise geometry by pressing the part onto the copper tape. As shown on Figure 4, the features were too small to be machined in our labs, which made this method difficult and would have been too expensive to outsource. Third, direct machining of the copper tape was also considered and tested, using a mill to cut out the geometry of the electrodes, as shown in Figure 4. This process was precise but left too many chips attached to the copper tape that could not be removed without damaging the type. After evaluating and trying some of these methods, the only cutting method left was to hand cut the tape in the desired geometry.

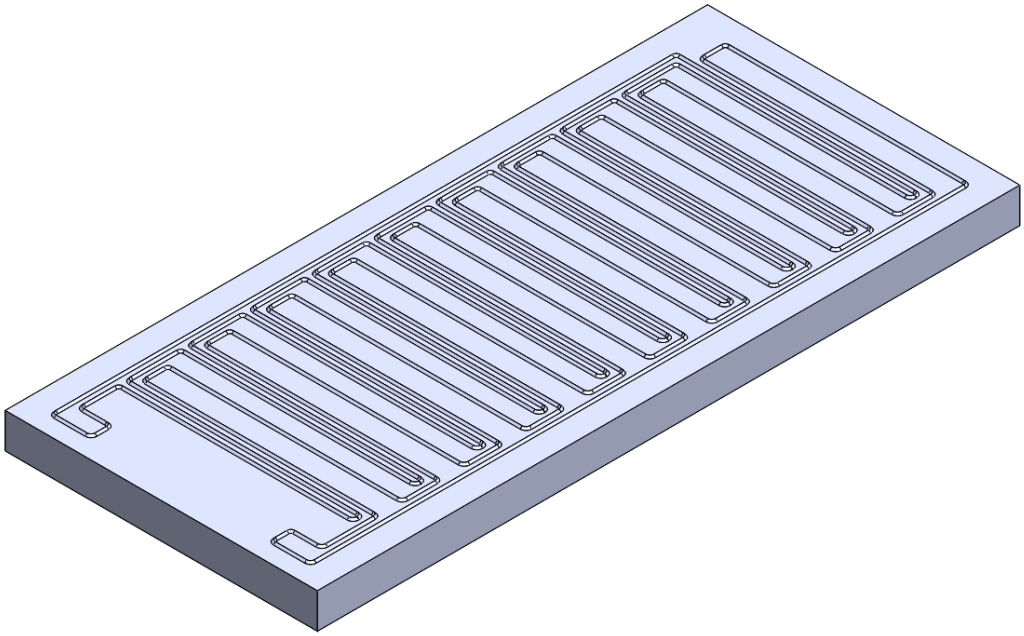

Figure 4: Cookie-cutter machined part for copper tape pump

For this cutting method, a plastic stencil was created and cut out by a laser-cutter which outlined the spacing between the electrode design. The stencil was placed on the copper tape and a razor was used to cut the electrode design out. Unfortunately, there were many sharp edges present and straight edges were difficult to achieve. Additionally, placing the copper electrodes on the substrate was difficult and not precise. The acrylic adhesive did not stick well enough to the substrate surface, so when the pump was flexed repeatedly, the electrodes peeled off at the flexural points. An additional Loctite 4203 prism adhesive was applied to improve adhesion between the electrodes and substrate, but sharp edges and dimensional accuracy remained a problem. An image of the copper tape macro-scale pump is shown below in figure 5:

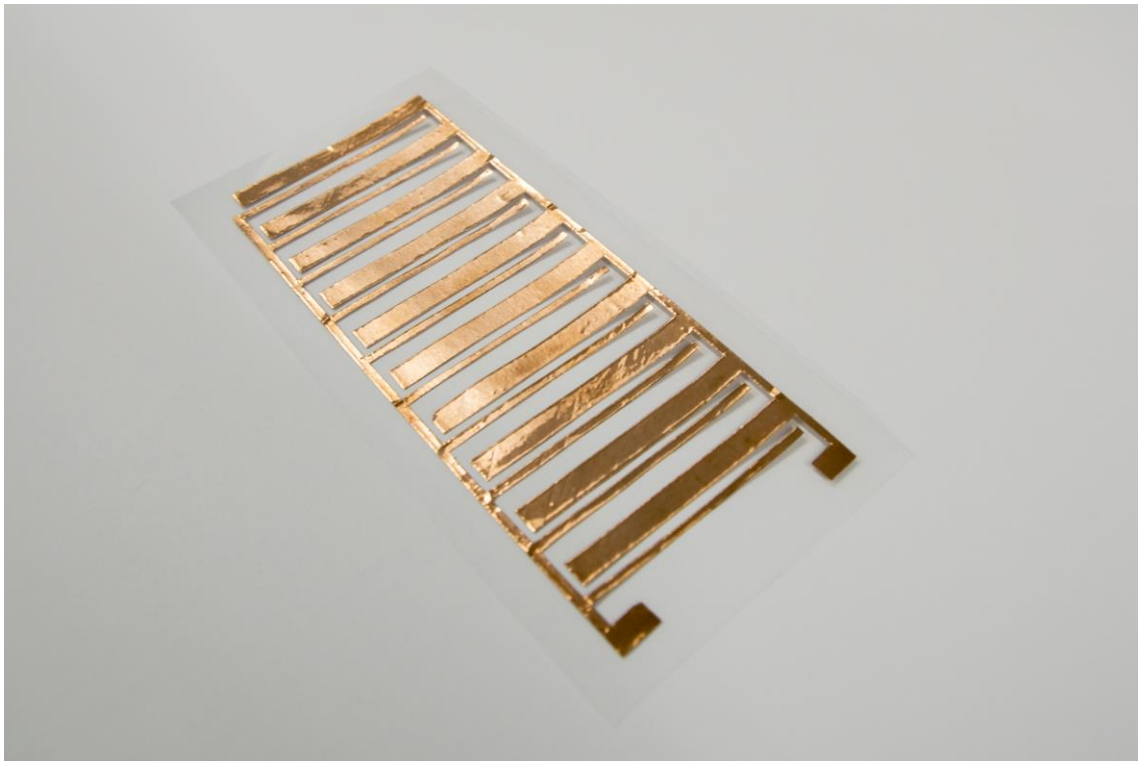

Figure 5: Copper tape macro-scale pump.

Screen Printed Prototypes

Based on the initial prototype, a better manufacturing method was necessary to ensure strong electrode and substrate bonding, ensure dimensional accuracy, and prevent sharp edges. The team considered several different manufacturing processes including chemical etching vapor deposition, and screen printing. None of these methods were easily available at WPI, therefore production of the pumps was outsourced to a local company called Techprint, which specialized in manufacturing printed electrical circuits. Techprint utilized a silk screen printing method to print the pumps. Screen printing is a printing technique which transfers ink onto a substrate except in areas blocked by a stencil. Ink is forced through a mesh by by a blade as it passes by. The substrate is a polyester PET film known as Melinex® manufactured by Dupont™. The ink, also manufactured by Dupont ™, is a conductive silver specially designed to strongly bond to the

Melinex® substrate. Both the resistivity and conductivity were similar in magnitude to those of previous materials used in EHD conduction experiments, but now flexible. The silver conductive ink had a resistivity of 3.81E-7 Ohm-m, and the polyester film had a resistivity of 1E17 Ohm-m.

The new pumps were designed on a flat plane to be able to pump a thin film. The pump can also be rolled, folded, or twisted into a desired geometric structure. The pump designs were created using the same design parameters as the macro-scale pump, in that the electrode ratios are the same. The characteristic length varies for each pump between the macro- and meso-scale. The original macro-scale pump was recreated with the same dimensions as the previous design. Four new pumps were created and named EHD Opposing Flow, Meso-Scale, Radial, and Nozzle along with the proof-of-concept EHD Macro Scale. Throughout the rest of this project report the designs will be referred to by these names. Images of these pumps are shown in Figure 6 below.

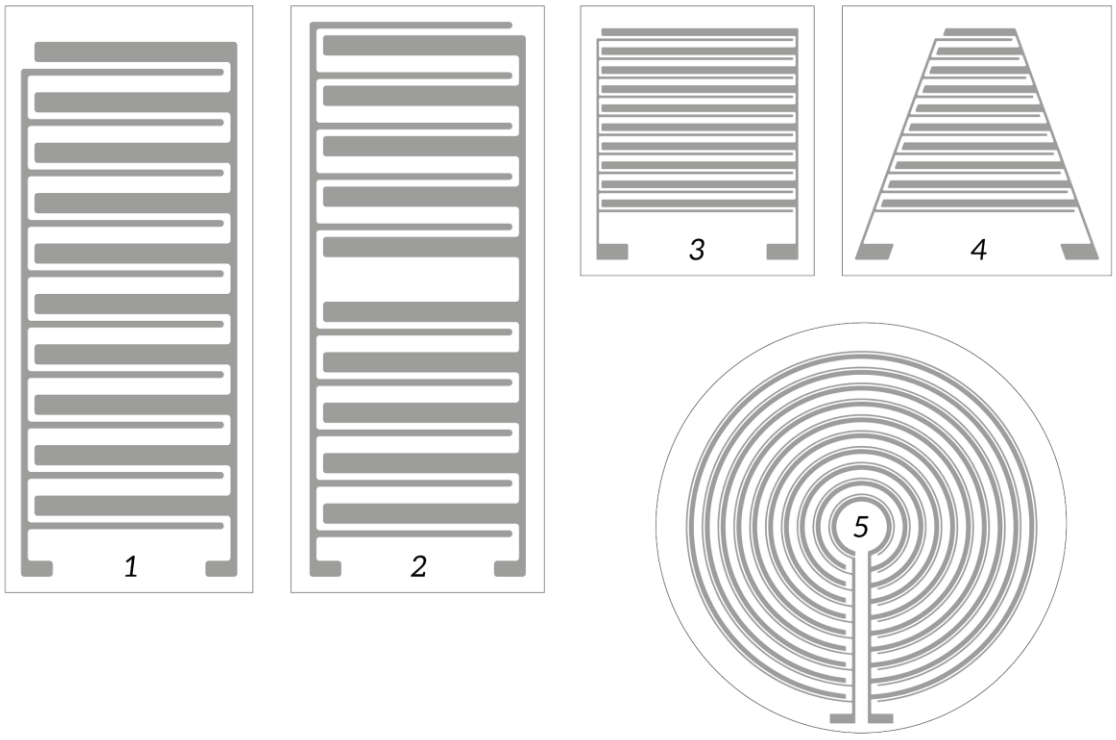

Figure 6: Pump designs (1) macro-scale pump, (2) opposing flows, (3) meso-scale pump, (4) nozzle, (5) radial.

The characteristic lengths are shown in Table 3, except for the radial pump. Unlike the four pumps shown in Table 3, the radial pump has a different ratio between electrodes and spacing. The radial pump has a high-voltage electrode size of 1.5d and an electrode pair spacing of 2.5d.

Table 3: Electrode characteristic lengths for each pump.

Pump	Macro	Macro Opposing	Meso	Nozzle
Characteristic Length, d	2.12	2.12	0.80	0.80

The characteristic length for each pump is the determining factor for how much voltage can be applied to the pump. A greater distance between the ground and high voltage electrode allows for more voltage to be applied. This is due to reaching the electrical breakdown limit for the dielectric working fluid, in this case corn oil. This electrical breakdown limit causes the actual fluid medium to completely ionize, rather than just the electrolytic impurities responsible for EHD phenomenon. For the Macro and Macro Opposing pumps, the maximum voltage achieved before breakdown is approximately 18kV. For the Meso and Nozzle pumps, the maximum voltage achieved before breakdown is approximately 10kV. The radial pump, with the smallest characteristic length, is limited to approximately 5kV before breakdown occurs.

Each of the five pumps served a different purpose in investigating different flows with different electrode designs. The Macro pump has been used in EHD conduction pumping to show heat transfer, mass transport, and smart flow control in thermal equipment, in the presence and absence of gravity (Siddiqui and Seyed-Yagoobi, 2009). The Opposing pump was designed to cause mixing of a fluid in the center of the pump. This would enhance the heat transfer experienced by the fluid if a heating component was placed in the center to give off heat and create a homogenous temperature. Like the Macro pump, the Meso pump was designed with

parallel electrodes but with a smaller characteristic length. The Meso pump was designed to compare the voltage intake and power consumption with that of the Macro pump. The electrode design of the Nozzle pump had not been explored before and was created to accelerate particles from large to small electrodes in a unique geometry. The pump was also able to be rolled into the shape of a nozzle and accelerate fluid through it.. The shape of the pump also allowed for it to fit into a conical geometry that could be used in a non-uniform diameter tube. Finally, the Radial pump was designed based on previous EHD conduction pumping experiments. The Radial pump is typically used in phase change situations were a heating component in the center is boiling away a coolant. This is especially prevalent in microgravity situations where boiling causes an insulative layer to form which must be replaced with liquid coolant to prevent a component from overheating.

Experiment Design

Initially, the experiment was thought to have a simple design that would incorporate the pump and a container to measure the velocity using pitot tubes. For this experiment we designed the following test environment for our pumps shown in Figure 7:

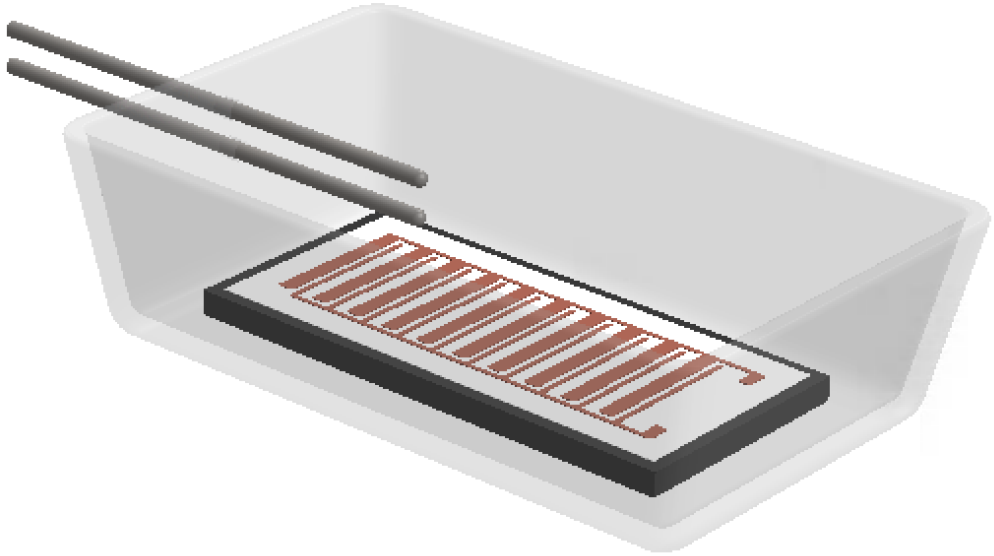

Figure 7: Experimental setup for pumps in a container with pitot tubes.

The design and setup for the experiment evolved with the different designs of the pump. It was known that the copper tape macro-scale pump was not going to achieve a high voltage, but a safe connection was still required. For safety conditions, the size of the testing chamber was increased from that shown in the previous figure. In this way, the pump was immersed in pure corn oil in a 64 quart transparent plastic bin. The transparency of the bin was essential for assuring the pump was completely submerged under the corn oil and for video recording of the experiments. If the pump was not submerged under the oil and exposed to the air, sparking will occur as air has a much lower breakdown voltage of about 3kV/mm. The copper tape macro pump was connected to a Glassman EH series high voltage supply capable of generating up to 30kV dc at low current. A small toothless alligator clip connector was used to connect the ground and high-voltage wires to the respective buslines on the pump. The alligator clips connectors needed to be filed down to ensure there were no sharp edges or charge injection could

occur. The voltage output was controlled with a potentiometer and breadboard connected to the high voltage supply. Images of the initial setup are shown in the Figure 8 and Figure 9 below.

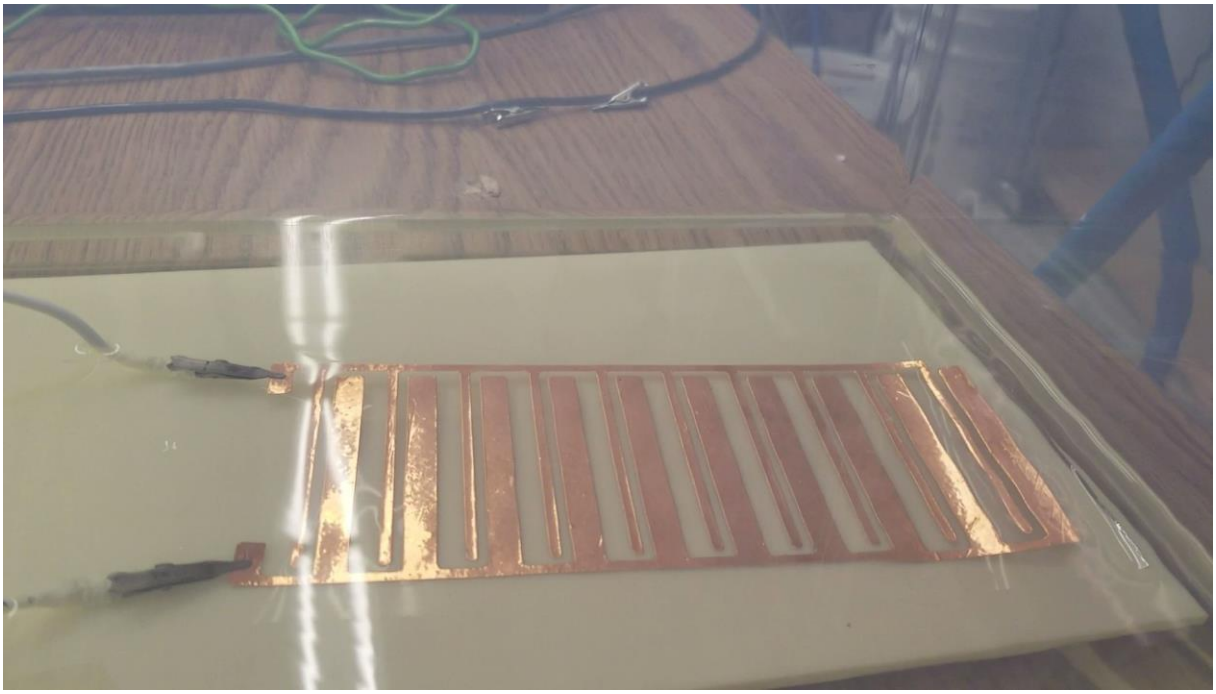

Figure 8: Copper-tape pump inside the testing chamber.

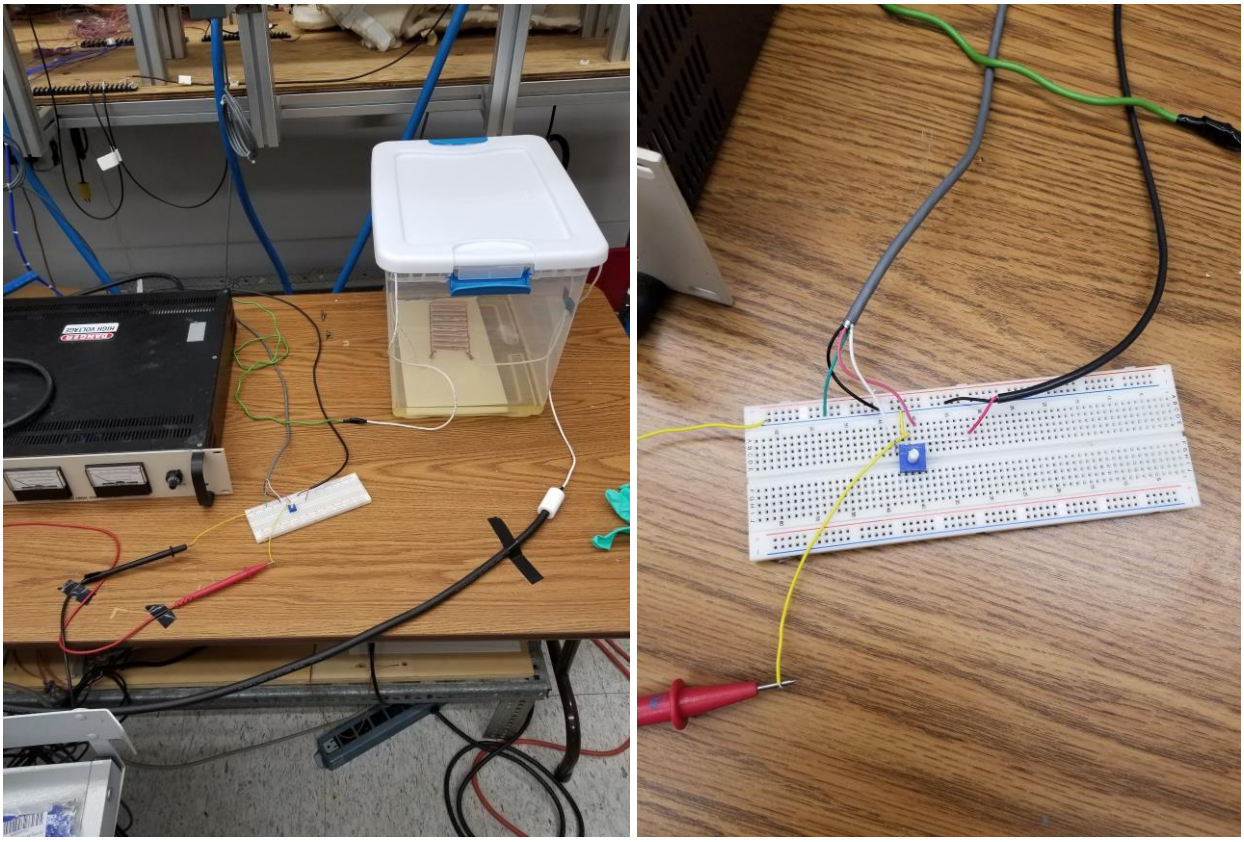

Figure 9: Initial setup for the potentiometer control of the voltage applied on the pumps.

There were a few major flaws with this preliminary experimental setup. First, controlling the voltage output manually with a potentiometer, on the order of kV, was potentially dangerous due to a lack of precision. The pump was also less dense than the corn oil so it would tend to float at or near the surface of the corn oil. Additionally, the flow the pump generated at higher voltages was enough to drag the pump through the tub. The alligator clip connectors used for this experiment also seemed to have some sharp edges even after being filed down, so charge injection occurred. Overall, without a safe and sound experimental setup, reliable data would not be able to be recorded, so changes were made.

Final Experimental Setup

The overall goal of the experiment was to collect data that can be used to measure the flow velocity across the five pumps. A National Instrument board (USB-6001) was used for data acquisition. Applied voltage and current were monitored continuously and recorded at each voltage. The LabVIEW program controlling the experiment automatically stopped the experiment from exceeding 2μA to ensure no sparking occurred, which is characterized by sudden spikes in current levels. Figures 10 and 11 shows the front panel and the block diagram of the LabVIEW program.

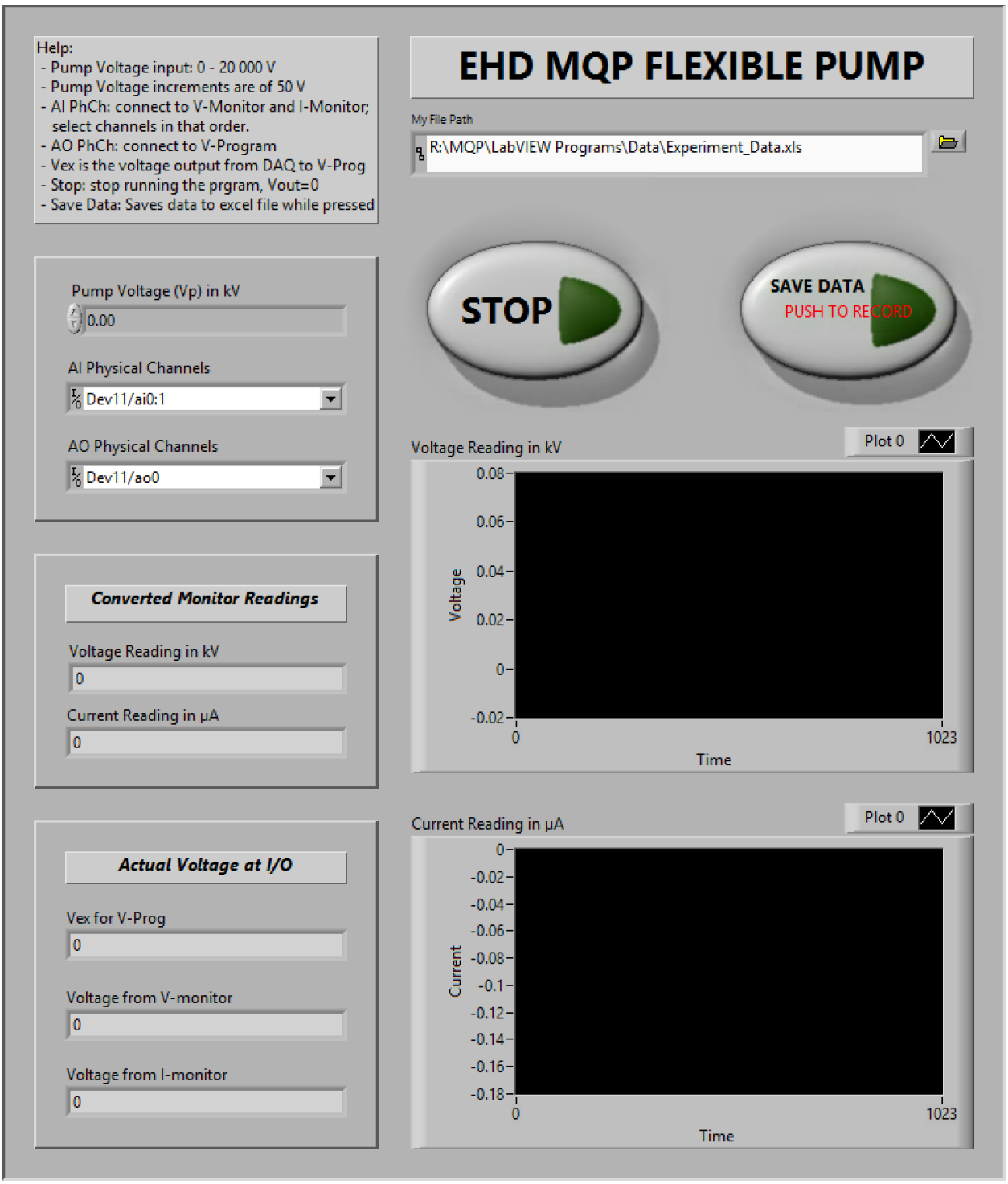

Figure 10: Front panel of LabVIEW program.

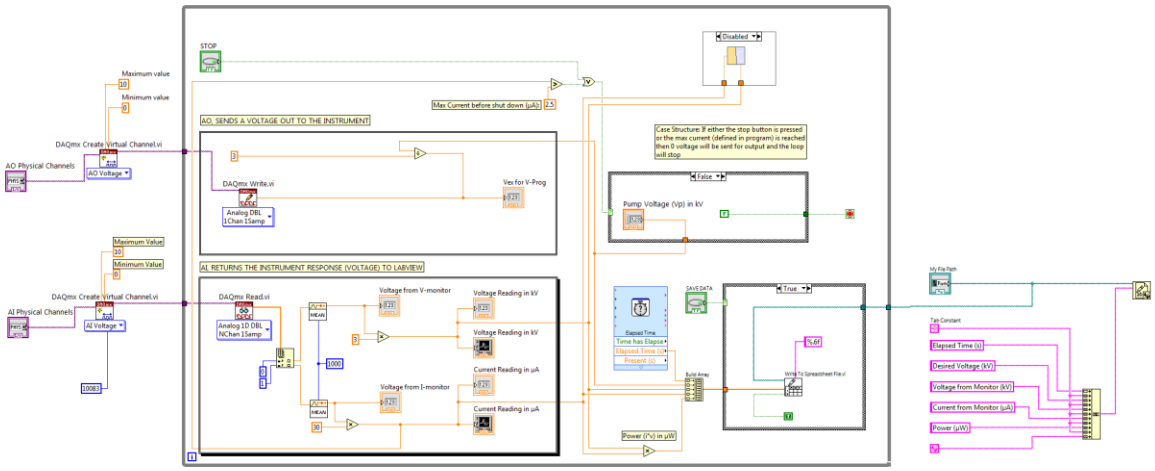

Figure 11: Block diagram of the LabVIEW program.

The plastic tub was chosen to prevent charge buildup for safety. The tub dimensions are 35 cm by 40 cm by 60 cm. Additionally, a 0.625 cm acrylic slab was placed at the bottom of the tub to further insulate the pump from the tub. Holes were drilled into the acrylic slab which secured fixtures designed for each pump to prevent movement of the pumps under their own pumping force. Fixtures for the pumps were 3D printed in either ABS or PLA to hold the pumps in various geometries. The 3D printed fixtures also incorporated tabs to hold down blade connectors for the buslines. The fixtures featured holes spaced 100mm apart such that all the fixtures could be fastened to the same bolts in the acrylic slab. This was deemed necessary in a proof of concept experiment to allow quick turnaround time between installations of each of the pump designs. Corn oil was selected as the working fluid for a similar reason, because it is easy to use, less toxic than refrigerants, and cheap to obtain, while maintaining the dielectric properties necessary. The corn oil working fluid has a dynamic viscosity of 52.3cP, dielectric breakdown of 12kV/mm, and resistivity of 1E10 Ohm-m. The apparatus is cleaned with isopropyl alcohol, and the corn oil is filtered through a 20µm-pore filter to prevent contamination

from foreign particles. All tests were conducted adiabatically at room temperature (21-25°C). Images of the 3D printed fixtures are shown below in Figure 12.

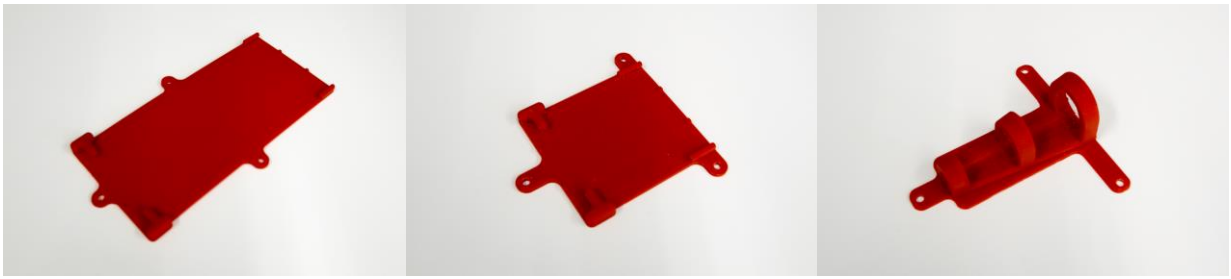

Figure 12: Left to right, macro flat, meso flat, and nozzle folded fixtures.

The velocity of the liquid was measured by capturing video from a top view of the tub. 40 -100µm PTFE particles were placed in the working fluid to visualize the flow. A transparent polycarbonate glass is used to cover the top of the tub and protect measurement equipment. Video was captured for the entire length of the pump. The video is then transferred to a computer where the timing of particles is recorded by counting the number of frames taken over the distance of several electrode pairs. Nine particles are randomly analyzed at each voltage and averaged to calculate the mean fluid velocity. The final experimental setup is shown below in Figure 13.

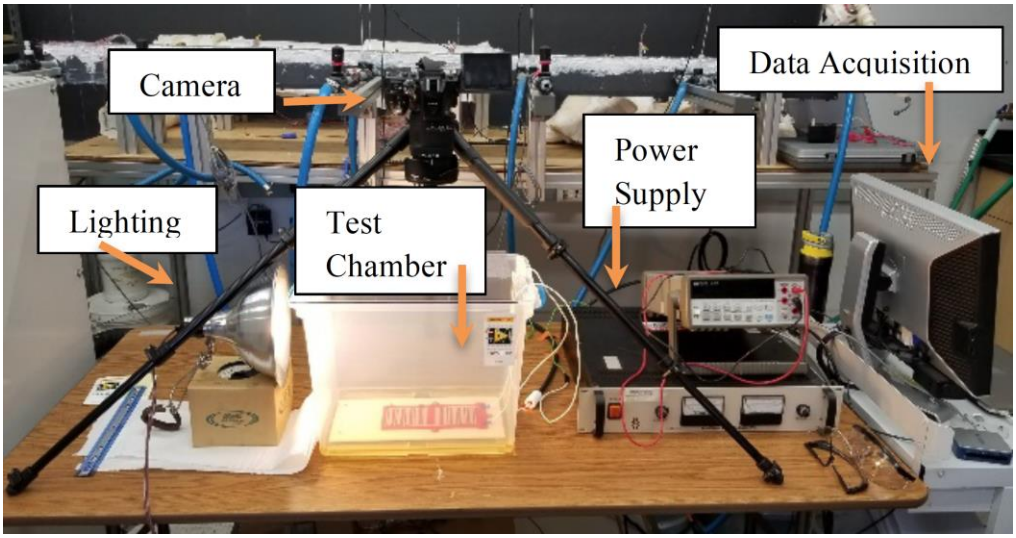

Figure 13: Final experimental setup.

Chapter 3: Results

Overview

This section shows the results of the data extracted from video footage of the experiments described in the previous section. A total of 9 particles from 3 different runs of each experiment are randomly selected. Utilizing the known distance across electrode pairs of the pump, the number of frames a particle takes to travel a given distance gives an accurate estimate of the velocity of the flow. It is important to note that the particles float on the surface of the thin film and therefore the film height makes a significant difference in the velocities measured. For the macroscale pumps, a film height of 5mm was used for all experiments. For the mesoscale pumps, a film height of 3mm was used for all experiments. Current measurements were captured through the DAQ box at each applied voltage during the experiment.

Due to the nature of these pumps being tested in an open system, using particles to estimate velocity was our only option. Pitot tubes would not be able to measure the thin film flows. Even in the flexed configurations, the velocity generated would not have given us accurate data using standard pitot tubes. Even expensive specialized pitot tubes might not have given us proper results. Therefore the data shown below is for each pump in their flat configurations pumping a thin film. The pumps were tested in their flexed configurations but accurate data could not be obtained.

Surface Velocity in Thin Film Configuration

The averaged results of the velocity measurements are shown in Figure 14 below. Measurements were taken at every 1kV, with the exception of the radial pump which was taken at every 0.3kV due to its smaller characteristic length compared to the other pumps. Velocities

are on the order of centimeters per second. The error bars represent one standard deviation from the average of the measurements.

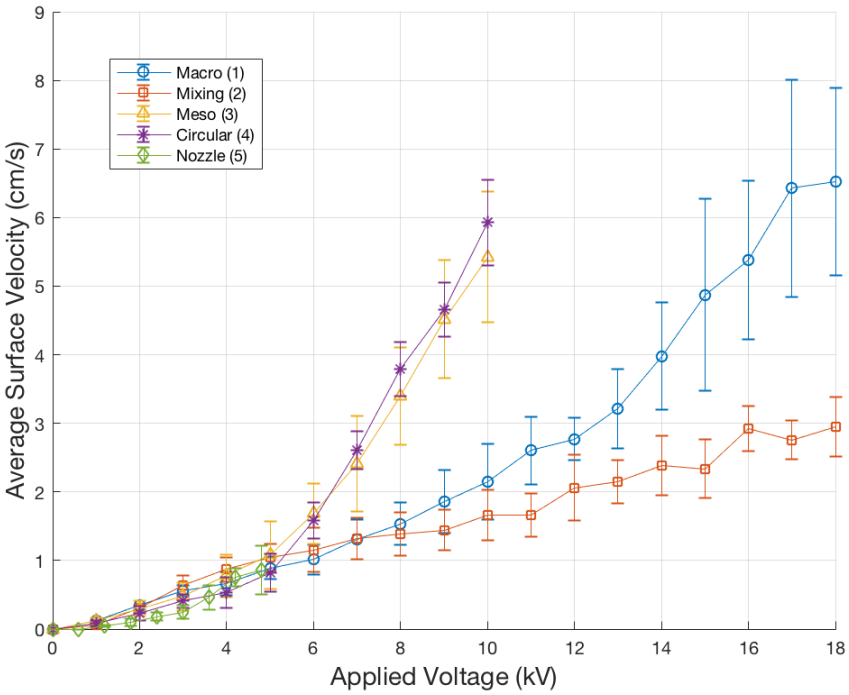

Figure 14: Liquid film average velocity versus applied voltage for each pump design.

Current and Electrical Power in Thin Film Configuration

The averaged results of the current measurements are shown in Figure 155 below. Figure 166 shows the electrical power consumption of the pump based on the applied voltage and the current measured. Current is on the order of micro-Amps and power is on the order of milli-Watts.

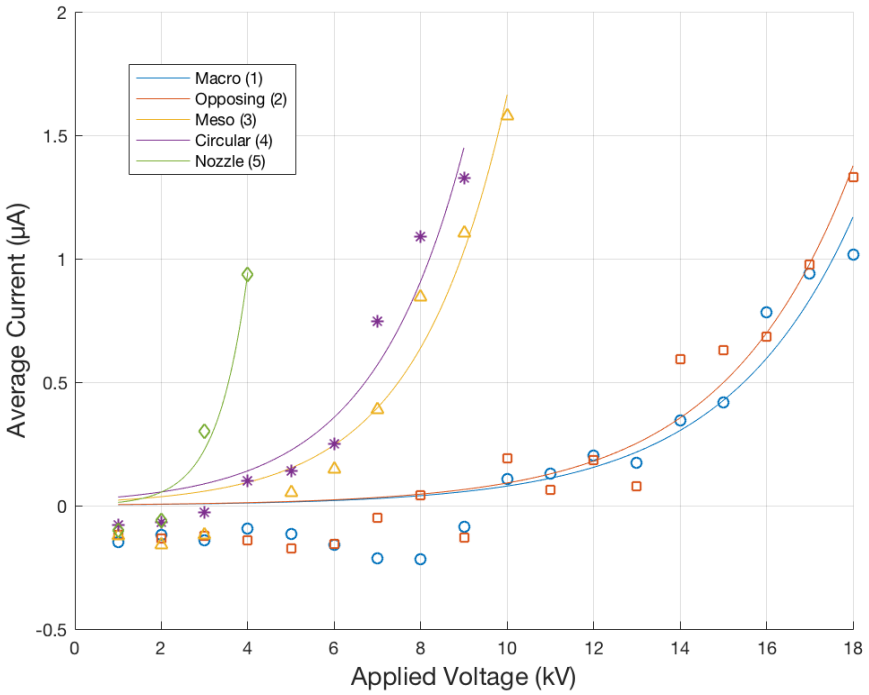

Figure 15: Current versus applied voltage for each pump design.

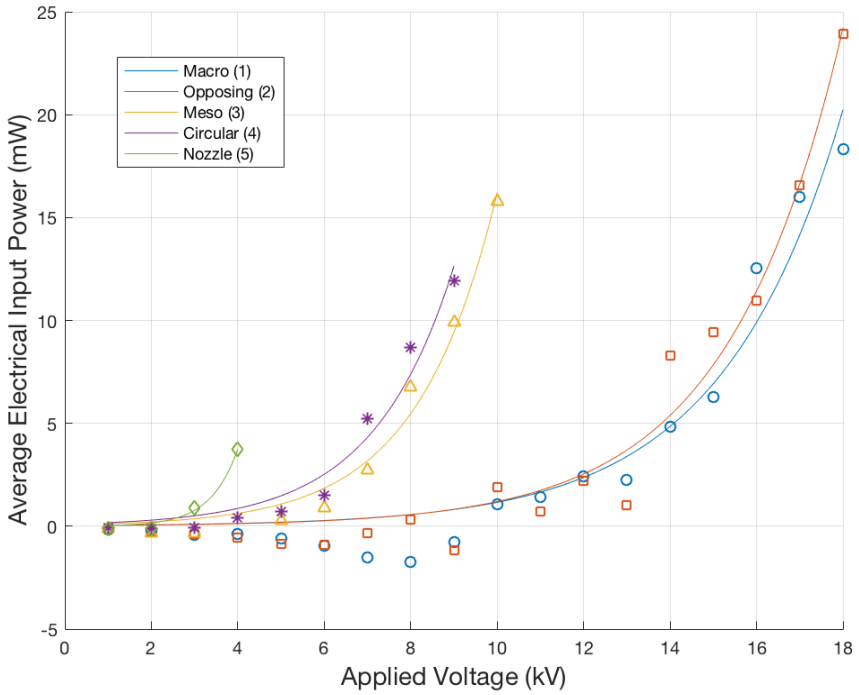

Figure 16: Electrical power consumed versus applied voltage for each pump design.

Chapter 4: Discussion

Overview

The flexible EHD conduction pumps designed and tested in this Major Qualifying Project were shown to have similar performance to previous rigid EHD pumps. The most significant issues encountered in the project were with the experimental setup itself rather than the pumps. An open system made collecting data on many pump configurations impossible, and thus data was only able to be collected by using particles and video recording in a thin film configuration. The pumps also required a second design iteration which solved the issue of interference with the buslines.

Important Results

The results of this project were collected from three runs of each pump in each configuration. The data from these tests shown above show similar performance to typical rigid EHD conduction pumps. These pumps are able to run at a similar maximum voltage prior to sparking. The current consumption of these pumps were also similar to what we would expect from rigid EHD conduction pumps of the same scale. We expected the performance of these pumps to be somewhat less due to the nature of printed electronics.

As seen in Figure 15 and Figure 16, the current and the power increase non-linearly with voltage. Comparing this to the velocities achieved, we could say that higher velocities will consume much more power than lower velocities. However, the voltage limit, established by the size of the electrodes, make the power never exceed the order of milli-watts. This proves that the pumps can achieve velocities on the order of 5 cm/s with just a power input on the order of 10 mW. In this way, the pumps can move fluid significantly fast with minimal power use.

The macro-scale pump designs generated significant flow, with the unidirectional design achieving a maximum average velocity of 6.52 cm/s at an applied voltage of 18kV. The opposing design achieved a maximum velocity of 2.94 cm/s at 18kV. These pumps were tested with a liquid film thickness of 5mm. It is expected that the opposing flow design would have about half the average velocity in a given direction due to the number of electrode pairs. The number of electrode pairs linearly increases the flow rate of the pump up to a certain point. The straight macro-scale pump has 10 electrode pairs in one direction, while the opposing macro-scale pump has 5 in either direction. In addition, the electrodes in the opposing macro-scale pump were working against one another, further reducing the velocity. The opposing pump did however have a unique characteristic: the film height was significantly reduced in the center, as shown in Figure 17.

(a)

(b)

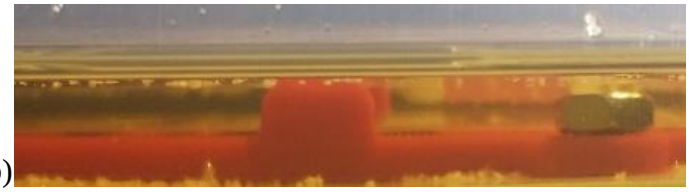

(c)

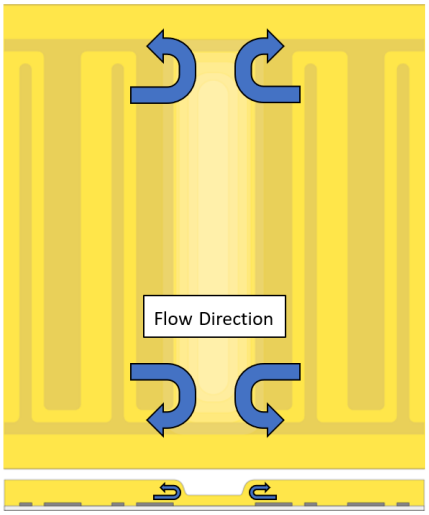

Figure 17: Mixing pump low pressure area, (a) angled view, (b) side view, (c) schematic of flow

This was due to the fluid recirculated on the surface of the tub, resulting in particles appearing to move in the opposite direction of the pumping force. This was a consequence of the open container environment rather than utilizing channels to direct flow. The macro-scale pumps in a semi-cylindrical and cylindrical geometry also generated similar flow velocities at the

surface of the working fluid. The semi-cylindrical design tended to cause a vertical circulation where fluid was pumped under the surface by the electrodes and then recirculated on the surface opposite the direction of the pumping force. The cylindrical pump was intended to create a circular flow around the tub. It was successful; however, the surface velocity was low due to the relatively small size of the pump compared to the volume of liquid in the tub container. The macro-scale pumps in their semi-cylindrical and cylindrical fixtures is shown below in figure 18.

(a) 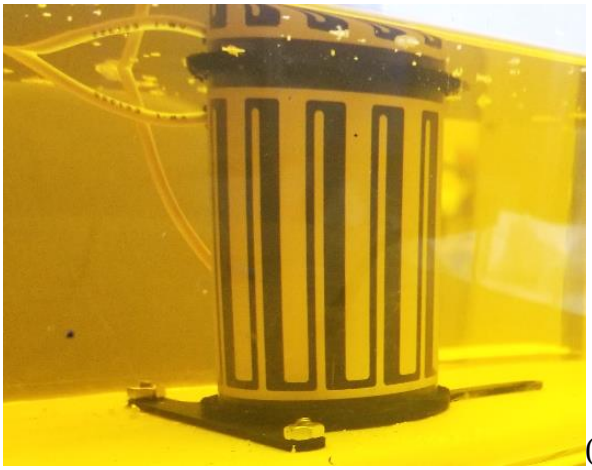 (b) 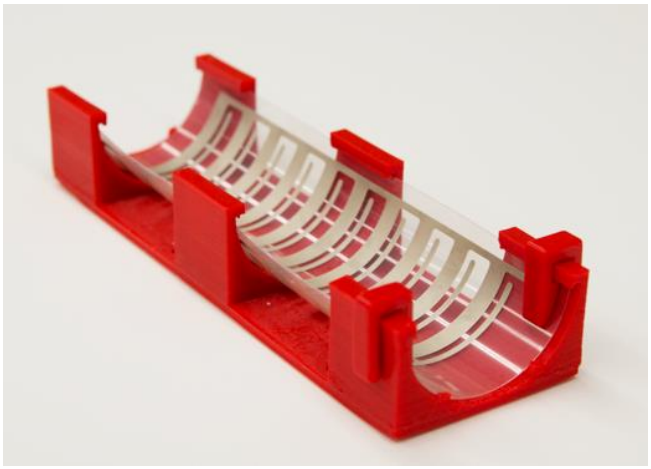

Figure 18: Macro-scale pump (a) wrapped cylindrically (b) flexed in semi-cylindrical configuration

The meso-scale pumps were tested at a liquid film thickness of 3mm and gave similar results to the macro-scale pumps. The maximum applied voltage for the straight meso-scale pump and nozzle pump reached 10kV compared to the radial pump, which reached 4.8kV because of the breakdown limitations of the radial pump's smaller characteristic length. For the same reason, the radial pump was tested in smaller voltage increments. Similar to the macro-scale pumps, the straight unidirectional meso-scale pump achieved a higher maximum velocity when compared to the radial pump which has opposing flows. The straight meso-scale pump achieved a maximum average velocity of 5.93 cm/s at 10kV. The nozzle pump in its flat

geometry had slight differences in its fixture, as shown in figure 19, namely that the sides of the pump are contained within walls on the fixture to create the nozzle. This prevent recirculation from the sides of the pump, unlike the other pump fixtures. The walls also resulted in significant acceleration of the particles similar to a traditional nozzle due to the decrease in cross-sectional area.

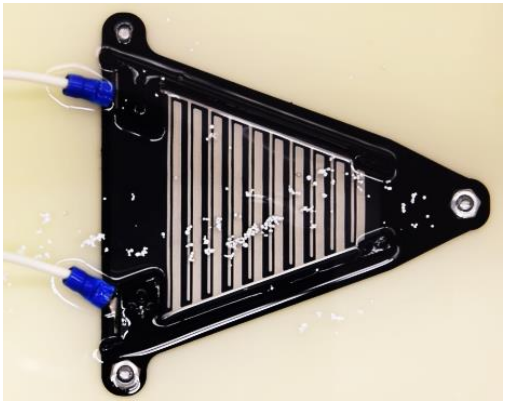

Figure 19: Nozzle pump in flat configuration

Prior to this project, there were no flexible pumps of any kind. These pumps serve as a proof of concept that flexible EHD conduction technology is feasible. They are cheaper to produce, and have some advantages over rigid pumps with very little performance loss compared to rigid EHD conduction pumps. These pumps will have a variety of applications ranging from deep space missions to terrestrial cooling system.

Issues Encountered

Some of the first issues encountered in this project were with the experimental setup. Connections to the high voltage power supply required several iterations. The high voltage line had to be resoldered several times to ensure there was no air trapped. This caused sparking several times at high voltage. The connections from the high voltage power supply to the pumps were initially flat clips which were filled down in order to prevent sharp edges from causing

charge injection into the working fluid. Even after filling these clips down, charge injection was still occurring. In order to address this issue we switched to blade connectors which would be held to the pumps using pressure from clips on the 3D printed fixtures. These clips were also filed down and did not introduce charge injection due to their simplified shape.

Another issue encountered with this project was with the testing methods. These pumps were envisioned to be able to be inserted into any setup and were tested in an open tub rather than a closed loop system. This lead to some issues with data collection as pitot tubes could not be used for flow field measurement. In order to acquire accurate data we used a camera to record the experiments from a top-down view and measured the time taken for particles to travel a specified distance across the pump. This was not without issues either. Due to the size range of the particles, some particles were slightly larger than the characteristic length of the electrodes. This caused some particles to interact abnormally with the flow field. This was not a significant issue for data collection, and the particles were instead crushed into a powder for future experiments.

Another prevalent issue was with the design and testing of the radial pump. Radial EHD conduction pumps are typically used in a phase-change type situation, where the fluid pumped into the center absorbs the heat from a source and vaporizes (Patel & Seyed-Yagoobi, 2017). In the case of this experiment, no phase change is occurring, and thus a mass transport issue occurs as the fluid pumped to the center cannot easily circulate out. This resulted in significant resistance to the generated flow. The smaller characteristic length also amplified the particle sizing issue described above.

The final issue encountered was with the single sided printing of the electrodes on the substrate. The bus lines were also printed on the same side and had an interaction with the

opposite polarity electrode. This tended to cause vortices and recirculation, especially on long term tests. This was addressed in another design iteration, where the electrodes were either moved to the opposite side of the substrate and connected with a thru hole or spaced significantly further away from the electrodes. This process would increase the cost of the manufacturing. However, it would fix the problem of the vortex generation between buslines and electrodes.

Impact

These flexible EHD pumps are the first of their kind and open up many possibilities for future improvement to technology. As previously mentioned, EHD conduction pumping technology is currently being tested on the International Space Station. Next generation satellites and missions to mars will require lightweight, reliable, and vibrationless cooling systems for their advanced electronics. These flexible pumps will also be ideal for soft robotics interacting with humans due to their ability to change shape with the dynamic movement of the robot. Pressure generation by these pumps can be used as an actuator by expanding and contracting bladders.

These pumps will also have terrestrial applications which can directly impact the lives of people. EHD conduction pumps are also able to be integrated into smart heat exchangers which can evenly distribute flow between parallel lines. This system can be automatic such that flow is adjusted to keep even temperature across all parallel lines to improve efficiency. These lightweight pumps could also be implement in future electric airplanes, or for cooling systems on electric vehicles due to their light weight.

A future goal is to implement EHD conduction pumps into vapor compression cycles to improve efficiency as mentioned in the introduction. These flexible pumps could potentially be used for their low cost in these systems to generate water from humid air for people that need it.

The significant advantage of these flexible pumps is that they are adaptable and can be used in many configurations and situations.

Final Designs

To address the problems that occurred for the initial pumps, new designs were created and finalized. TechPrint and the same silk-screen printing method was used for the final design iteration of the pumps. Two new designs were created for each of the five pumps which addressed the close proximity of the buslines to the electrodes which induces and unintended electrical field. In the first design, the buslines were placed on the opposite side of the substrate from the electrodes. The buslines were connected to their respective electrodes by utilizing a through hole. It was ensured that the through holes would not create any sharp edges which would result in charge injection. This made certain that the buslines would not interact with the electrodes and create a strong electric field between them.

The second final design for the five pumps kept the buslines on the same side as the electrodes but separated the buslines and electrodes from each other by simply increasing the distance between them. The distance was increased so a strong electrical field was not induced by the buslines because of its close proximity with the electrodes. The electrode designs from the previous designs were maintained, except for the Nozzle. The Nozzle electrodes were originally rectangular in shape and were most ideal for the flat configuration. Rectangular electrodes were not ideal for the nozzle in a conical shape however. Therefore, the electrodes were changed to be radial, similar to the Radial Pump, such that the electrodes would be directed to the tip of the nozzle around the entire pump. The distances for each of the five pumps is shown in Table 4 below. Unfortunately, they could not be tested together with the other pumps for this project.

Drawings of the designs and pictures of the actual manufactured pumps can be found on Appendix B.

Table 4: Electrode characteristic lengths for each final screen printed pump.

Pump	Macro	Radial	Meso	Nozzle
Characteristic Length, d	2.12	0.80	0.80	0.80

Conclusion

Flexible EHD conduction pumping technology has been shown to have similar performance to existing rigid EHD conduction pumps. The goal of this project, to prototype and test flexible EHD conduction pumps, was achieved. The pumps were able to generate flow velocities on the order of 6 cm/s at maximum voltage in the open system. These pumps are able to be flexed into different shapes and continue functioning as intended. This project serves as a proof of concept for flexible EHD conduction pumping. Future work would be able to test additional pumping geometries under varying conditions as well as in dynamic situations. These flexible pumps also will be tested at micro scale. Though more testing is required, this project proves that flexible EHD pumping technology is feasible with great potential applications.

References

Atten, P., and Seyed-Yagoobi, J. (2003). Electrohydrodynamically Induced Dielectric Liquid Flow through Pure Conduction in Point/Plane Geometry. *IEEE Transactions On Dielectrics And Electrical Insulation*, Vol. 10.1.

Atten, P., and Seyed-Yagoobi, J. (1999). Electrohydrodynamically induced dielectric liquid flow through pure conduction in point/plane geometry-theory. *Dielectric Liquids, 1999. (ICDL '99) Proceedings of the 1999 IEEE 13th International Conference.*

Feng, Y., and Seyed-Yagoobi, J. (2006). Control of liquid flow distribution utilizing EHD conduction pumping mechanism. *IEEE Transactions on Industry Applications*, Vol. 42.

Jeong, S., & Seyed-Yagoobi, J. (2004). Fluid circulation in an Enclosure Generated by Electrohydrodynamic Conduction Phenomenon. *IEEE Transactions on Dielectrics and Electrical Insulation*, Vol. 11.5.

Jeong, S., Seyed-Yagoobi, J., and Atten, P. (2003). Theoretical/Numerical Study of Electrohydrodynamic Pumping through Conduction Phenomenon. *IEEE Transactions On Industry Applications*, Vol. 39.2.

Louste, C., Artana, G., Moreau, E., & Touchard, G. (2005). Sliding Discharge in Air at Atmospheric Pressure: Electrical Properties. *Journal of Electrostatics*, Vol. 63.

Melcher, J.R. (1981). *Continuum Electromechanics.* Cambridge, MA: MIT Press

Patel, V., & Seyed-Yagoobi, J. (2014). Recent Experimental Advances in Electrohydrodynamic Conduction Pumping Research. *2014 IEEE Industry Application Society Annual Meeting*.

Patel, V., & Seyed-Yagoobi, J. (2011). Dielectric Fluid Flow Generation in Meso-tubes with Micro-scale Electrohydrodynamic Conduction Pumping. *2011 IEEE International Conference on Dielectric Liquids*.

Patel, V.K. and Seyed-Yagoobi, J, "A mesoscale electrohydrodynamic-driven two-phase flow heat transport device in circular geometry and in-tube boiling heat transfer coefficient under low mass flux", Journal of Heat Transfer, 137(4), p.041504 (2015).

Patel, V.K. and Seyed-Yagoobi, J., "Combined Dielectrophoretic and Electrohydrodynamic Conduction Pumping for Enhancement of Liquid Film Flow Boiling", ASME Journal of Heat Transfer, Vol. 139, pp. 061502-1 (2017).

Pearson, M.R., and Seyed-Yagoobi, J. (2013). EHD Conduction-Driven Enhancement of Critical Heat Flux in Pool Boiling. *IEEE Transactions on Industry Applications*, Vol. 49.

Pearson, M.R., & Seyed-Yagoobi, J. (2013). "Electrohydrodynamic Conduction Driven Single- and Two-Phase Flow in Microchannels with Heat Transfer." *ASME Journal of Heat Transfer*, Vol. 135.

Seyed-Yagoobi, J. (2005). Electrohydrodynamic Pumping of Dielectric Fluids. Elsevier, Journal of Electrostatics, Vol. 63.

Siddiqui, M.A. and Seyed-Yagoobi, J. (2009). Experimental study of pumping of liquid film with electric conduction phenomenon. *IEEE Transactions on Industry Applications*, Vol. 45..

Stuetzer, O. (1959). Ion Drag Pressure Generation. *Journal of Applied Physics*. Vol. 30.

Taslak, E., Kocatepe, C., Arikan, O., & Kumru, C.. "Electrical Analysis of Corn Oil as an Alternative to Mineral Oil in Power Transformers." IJEPE, vol. 9.8, pp. 873-877 (2015).

Hanaoka, R., Nakamichi, H., Takata, S., & Fukami, T, "Distinctive Flow Properties of Liquid Jet Generated by EHD Pump and Conical Nozzle", Electrical Engineering In Japan, vol. 154.1, pp. 9-19 (2005).

Bedell, S. W., Shahrjerdi, D., Fogel, K., Lauro, P., Bayram, C., Hekmatshoar, B., . . . Sadana, D. (2014). Advanced flexible electronics: Challenges and opportunities. Paper presented at the Micro- and Nanotechnology Sensors, Systems, and Applications Conference, 9083 90831G-90831G-9. doi:10.1117/12.2051716

Chang, J., Ge, T., & Sanchez-Sinencio, E. (2012). Challenges of printed electronics on flexible substrates. Paper presented at the 582-585. doi:10.1109/MWSCAS.2012.6292087

Wong, W. S., Salleo, A., & Springer Books. (2009). *Flexible electronics: Materials and applications* (1. Aufl. ed.). New York: Springer. doi:10.1007/978-0-387-74363-9

Wu, Z., Huang, Y., & Chen, R. (2017). Opportunities and challenges in flexible and stretchable electronics: A panel discussion at ISFSE2016. Micromachines, 8(4), 129. doi:http://dx.doi.org.ezproxy.wpi.edu/10.3390/mi8040129

APPENDIX A: Drawing of Copper Tape Prototype

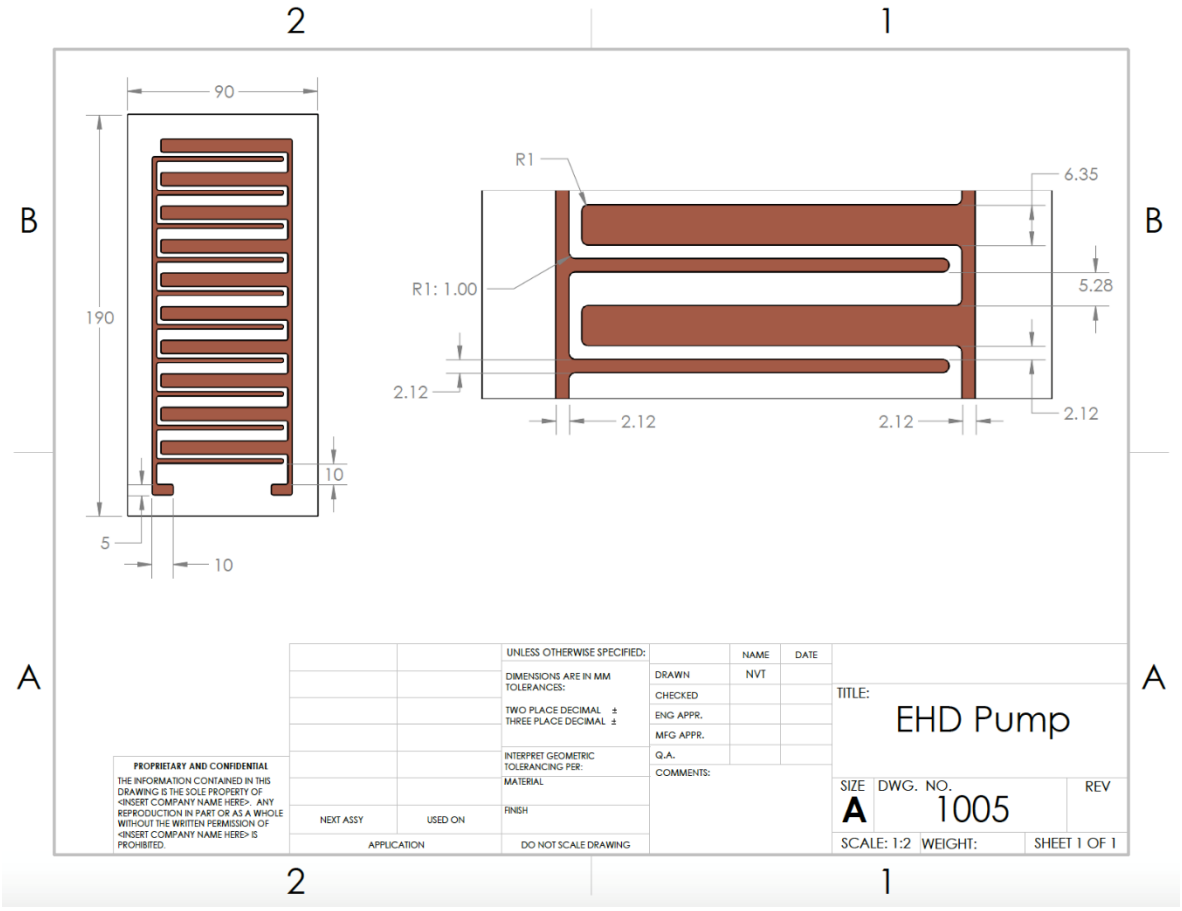

APPENDIX B: Initial Pump Designs

Macro-scale pump

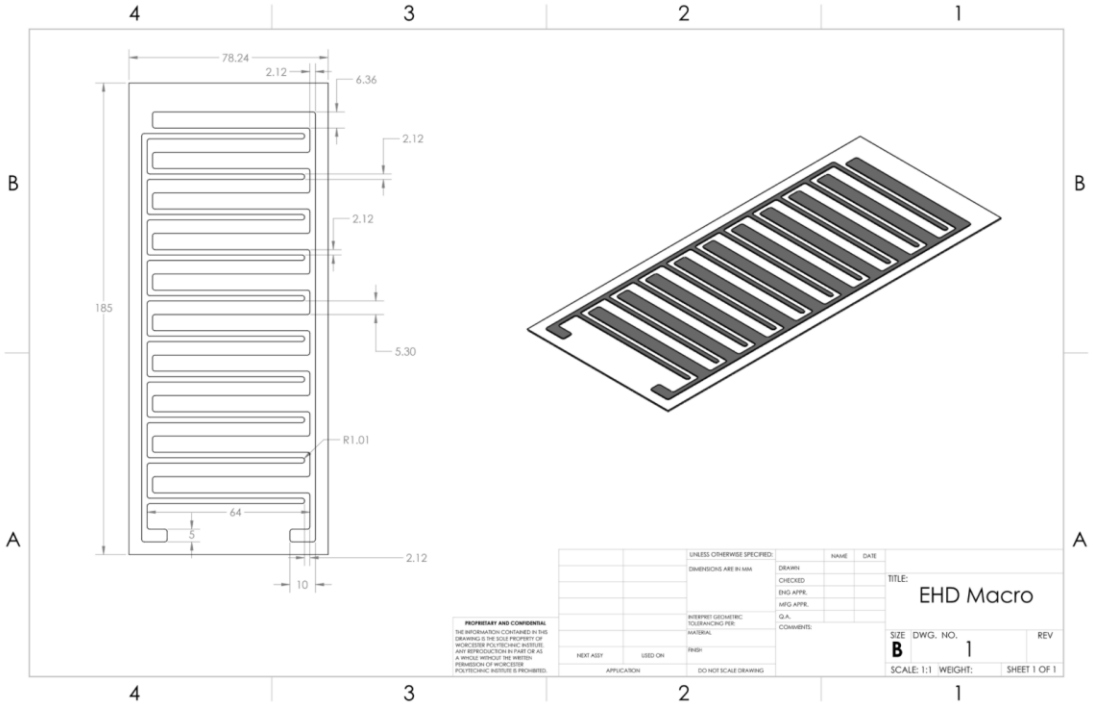

Meso-scale pump

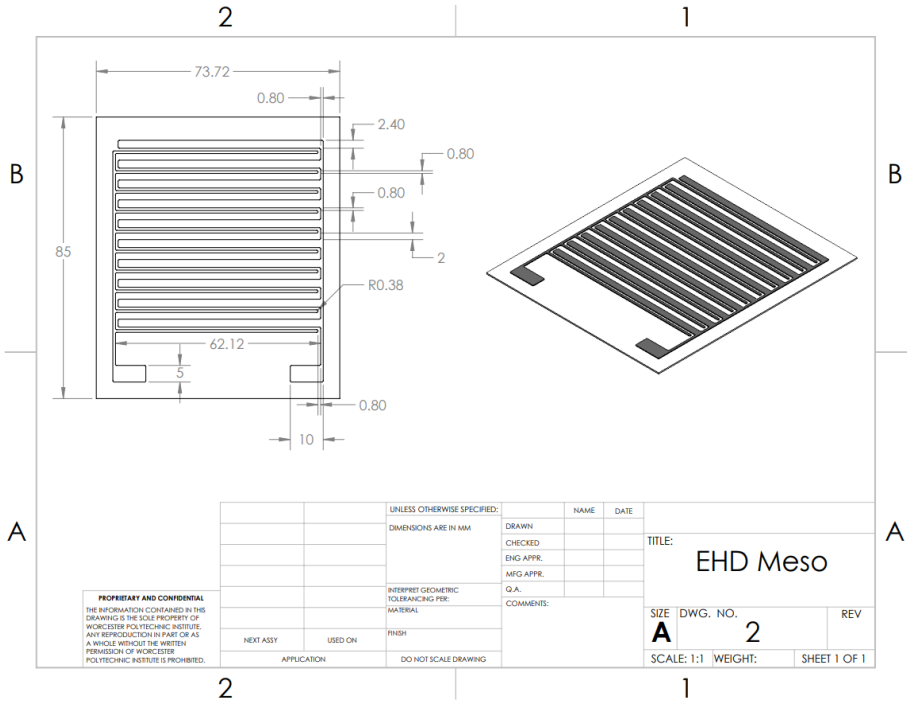

Nozzle pump

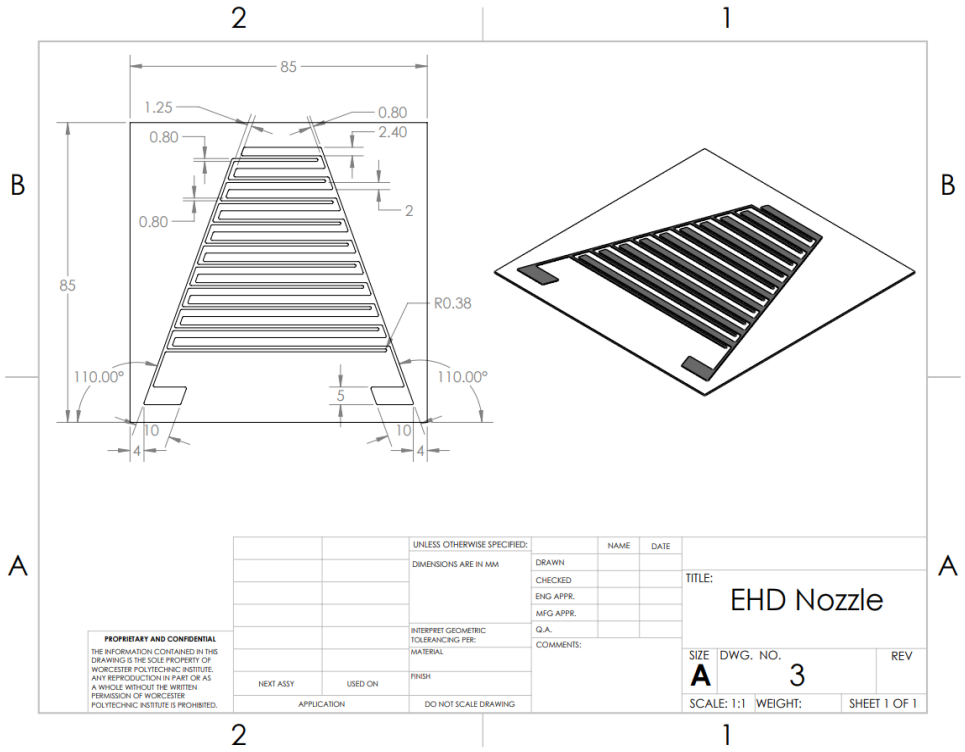

Radial pump

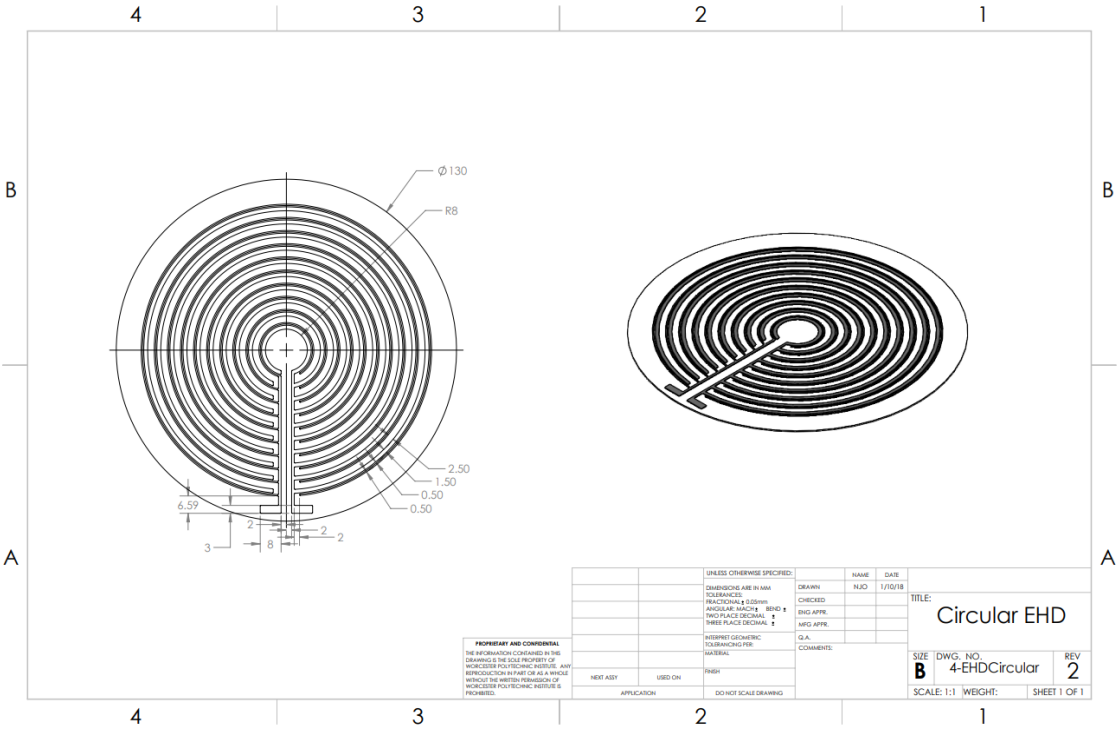

Opposing-flow pump

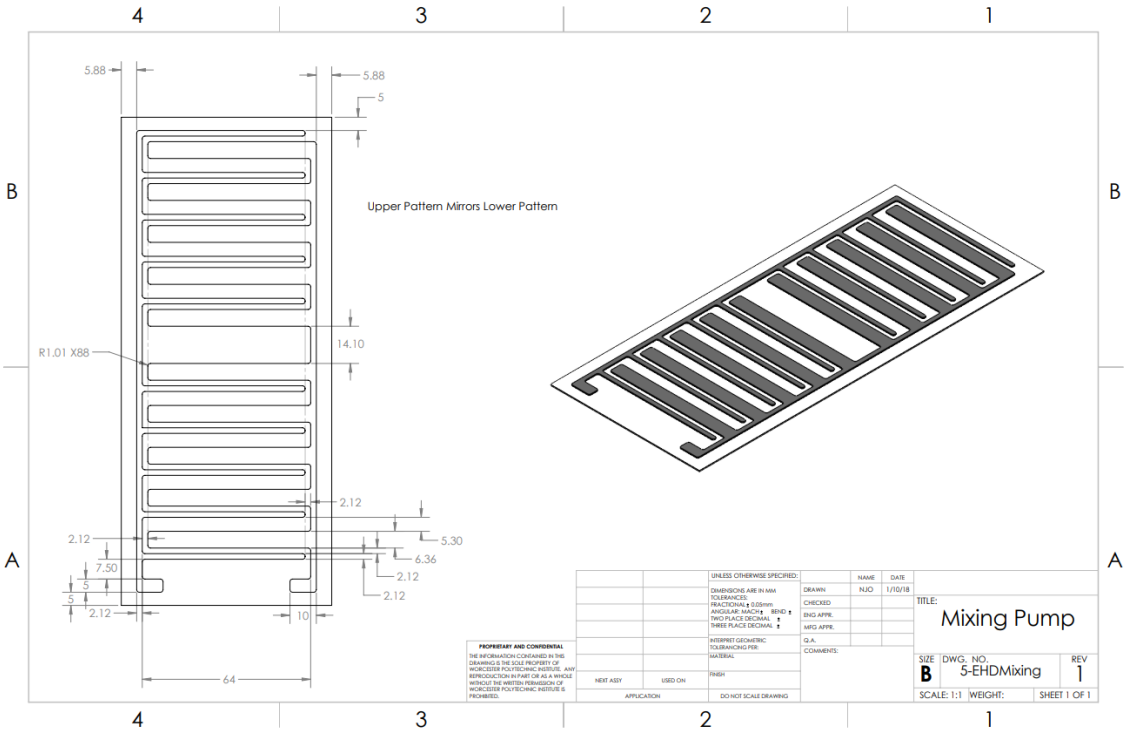

APPENDIX C: Final Pump Designs Drawings

Macro-Scale Pump (Single and Double Sided)

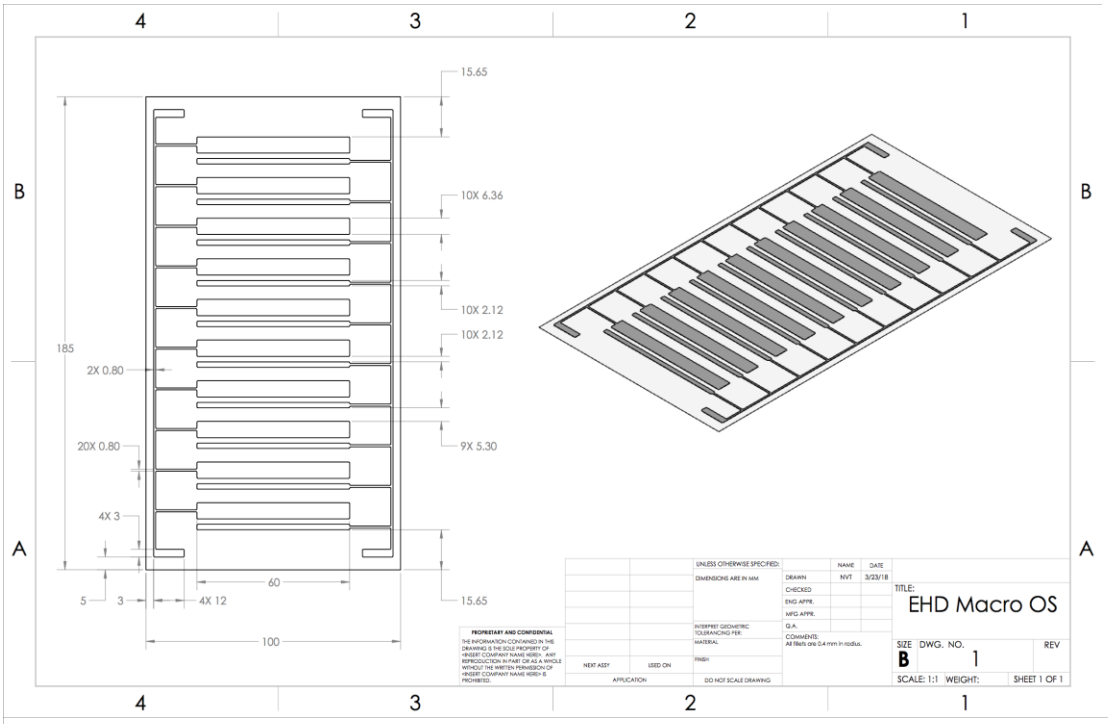

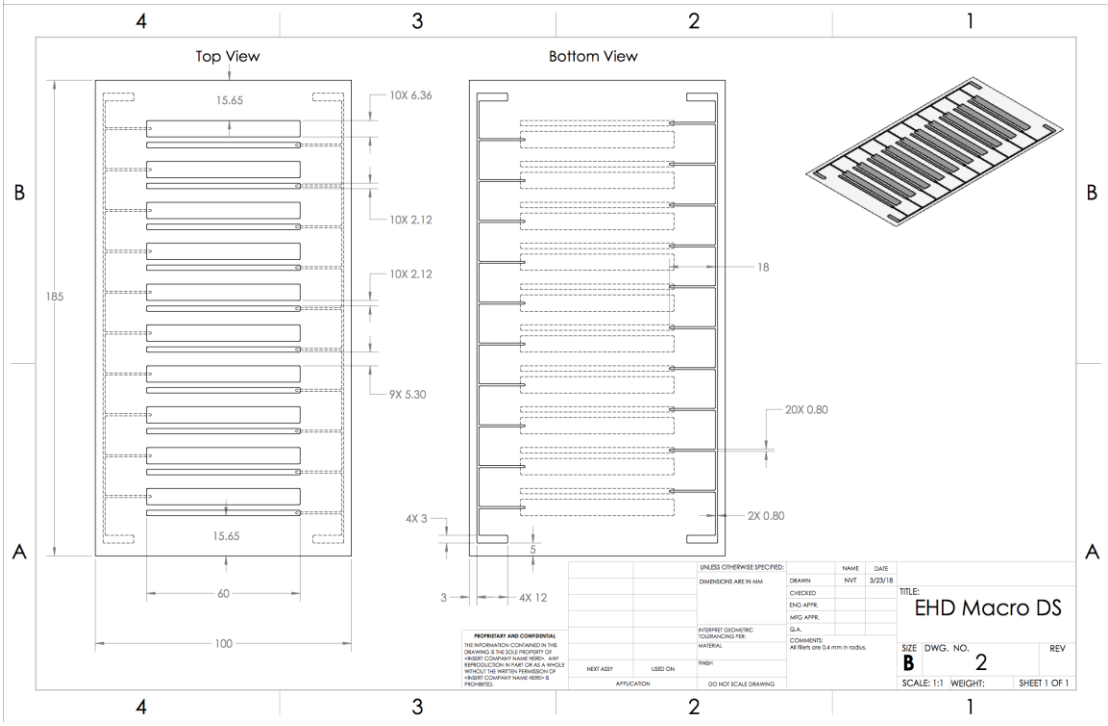

Meso-Scale Pump (Single and Double Sided)

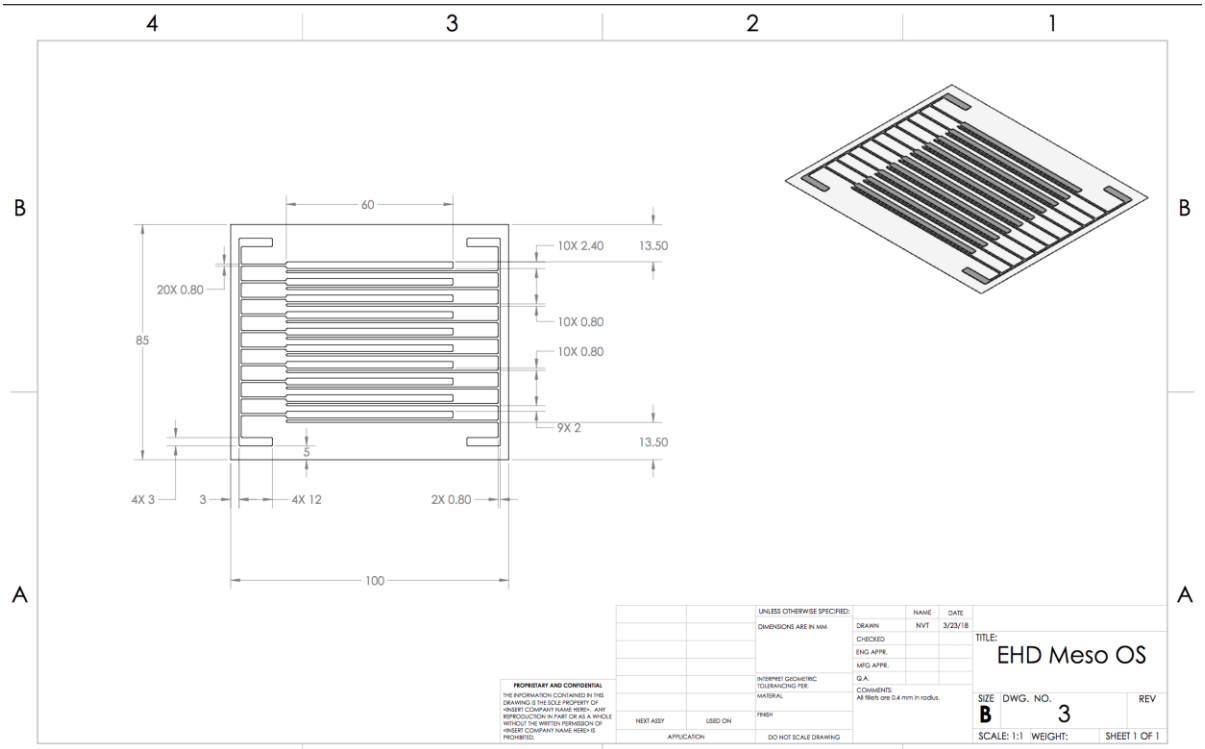

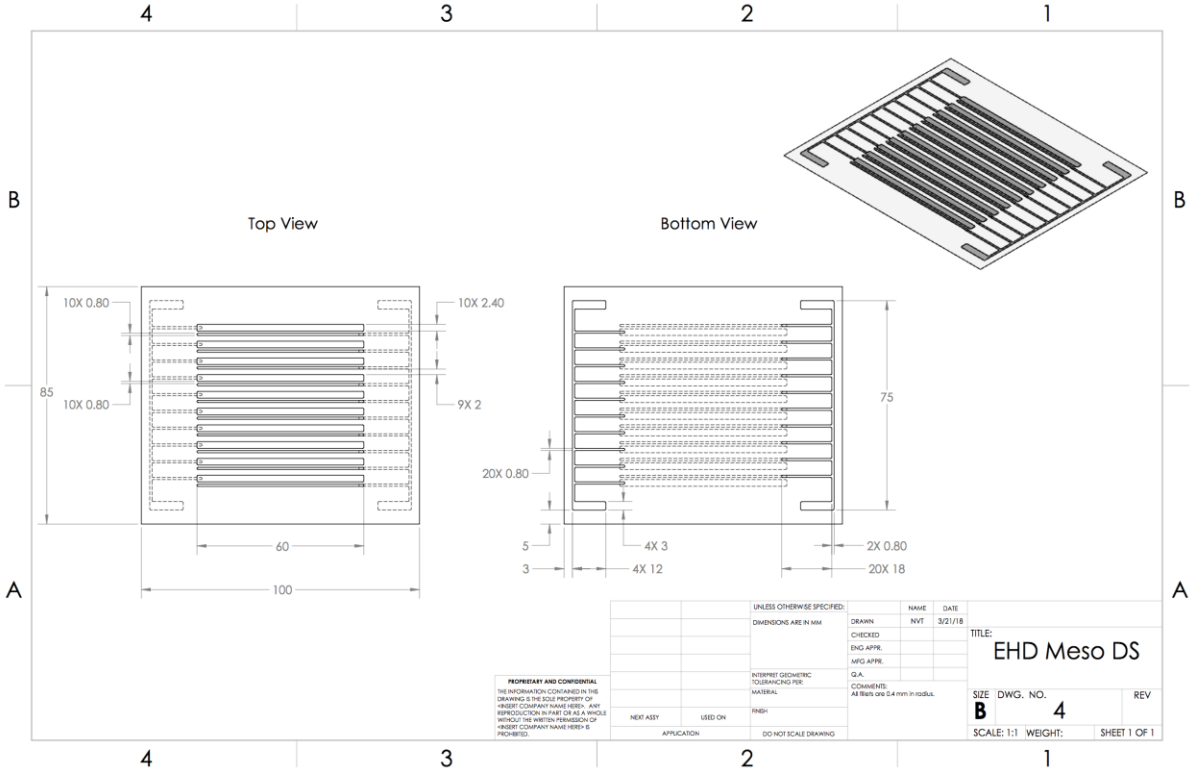

Nozzle Pump (Single and Double Sided)

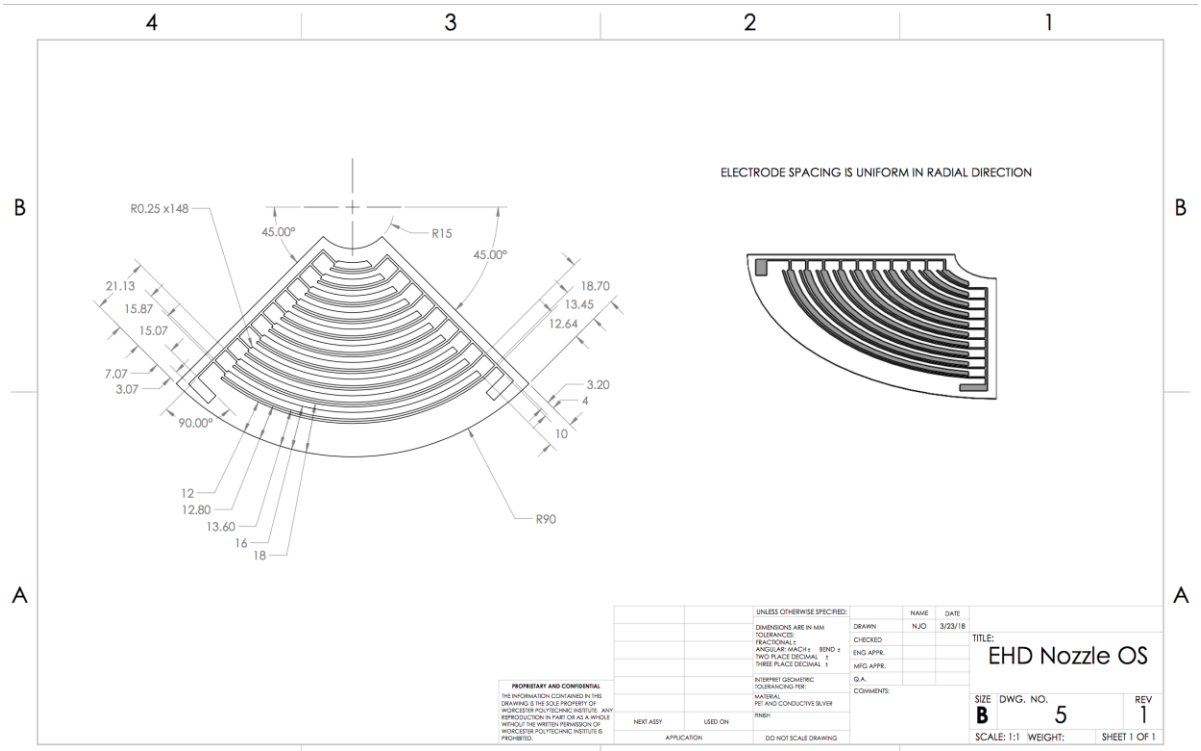

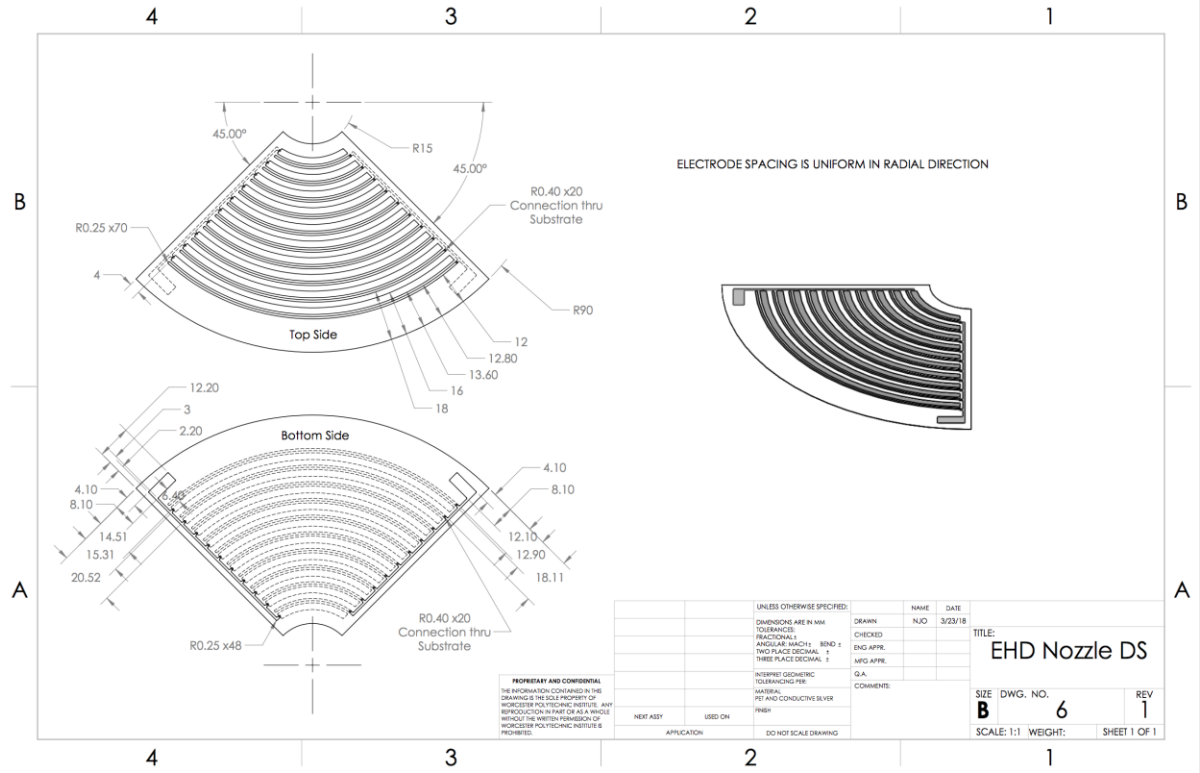

Radial Pump (Single and Double Sided)

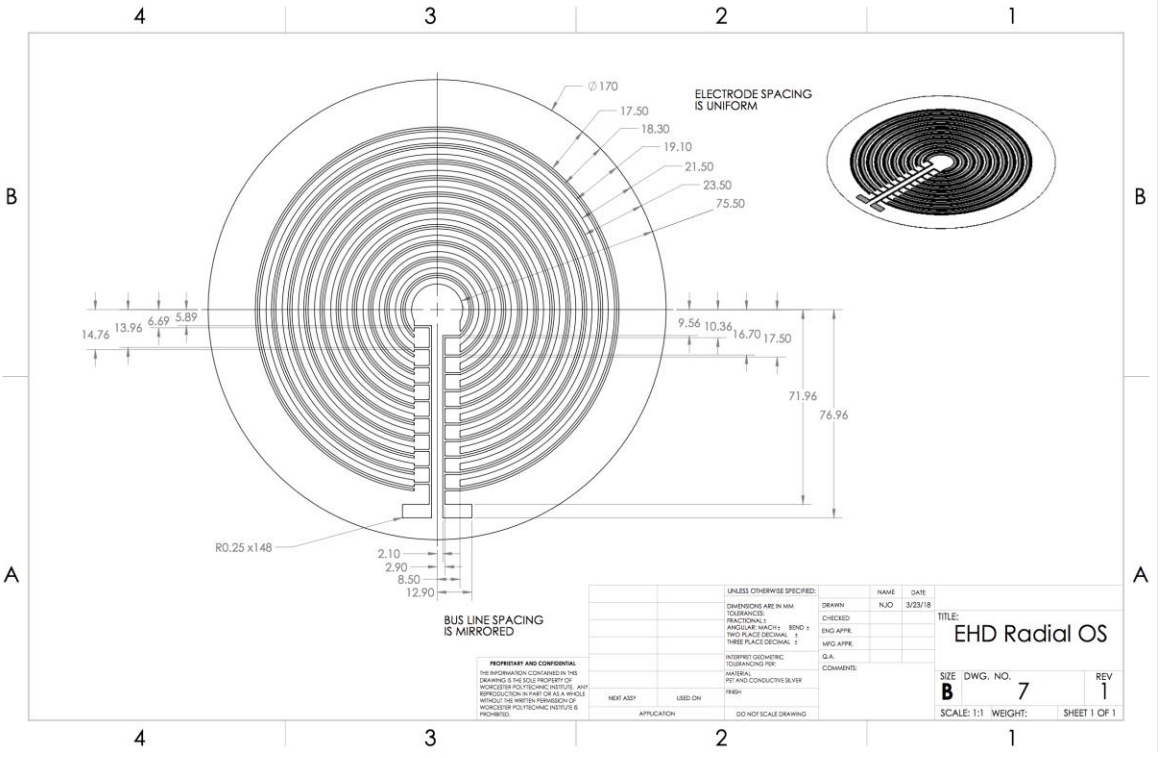

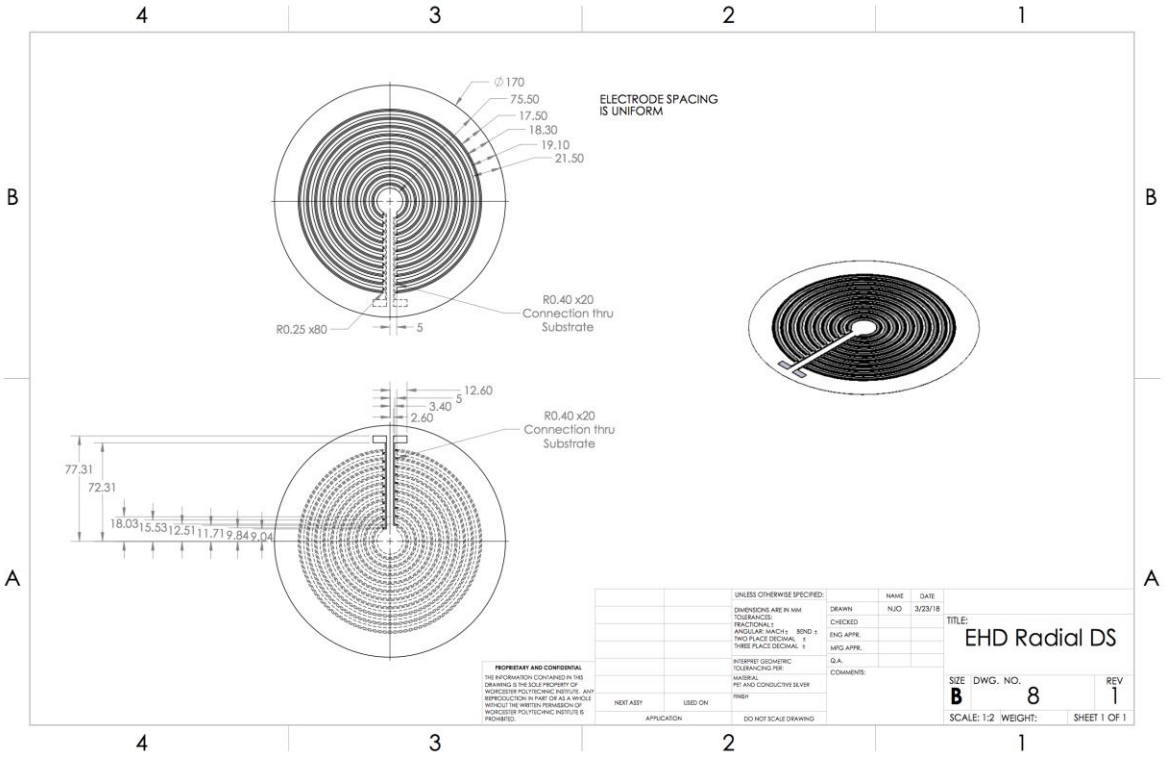

APPENDIX D: Final Pump Designs Pictures

Macro-scale pump

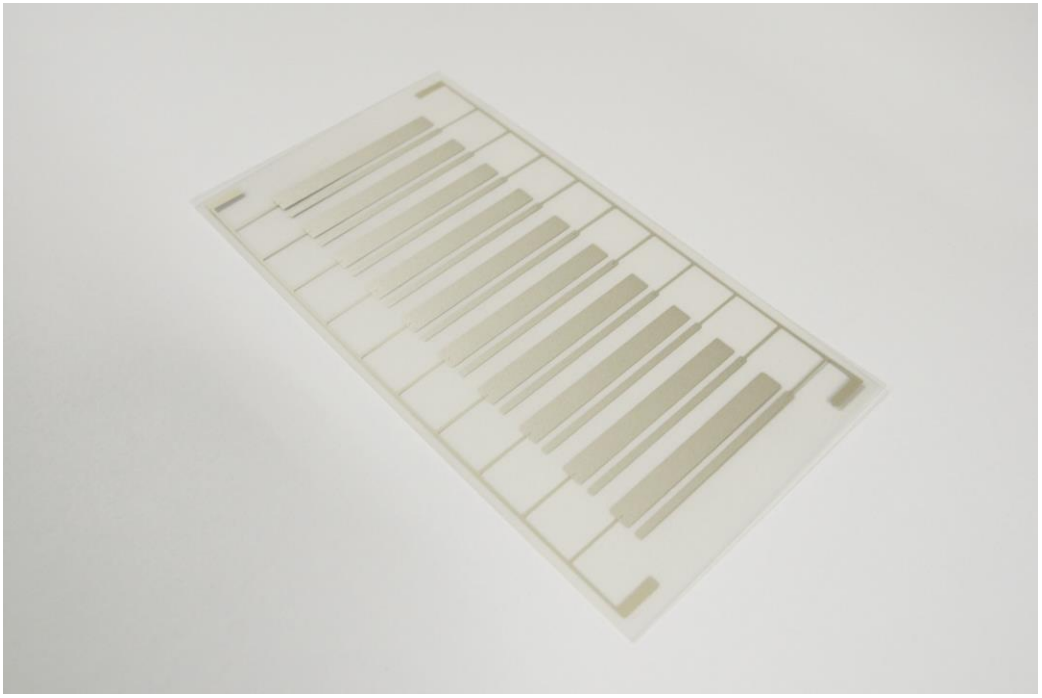

Meso-scale pump

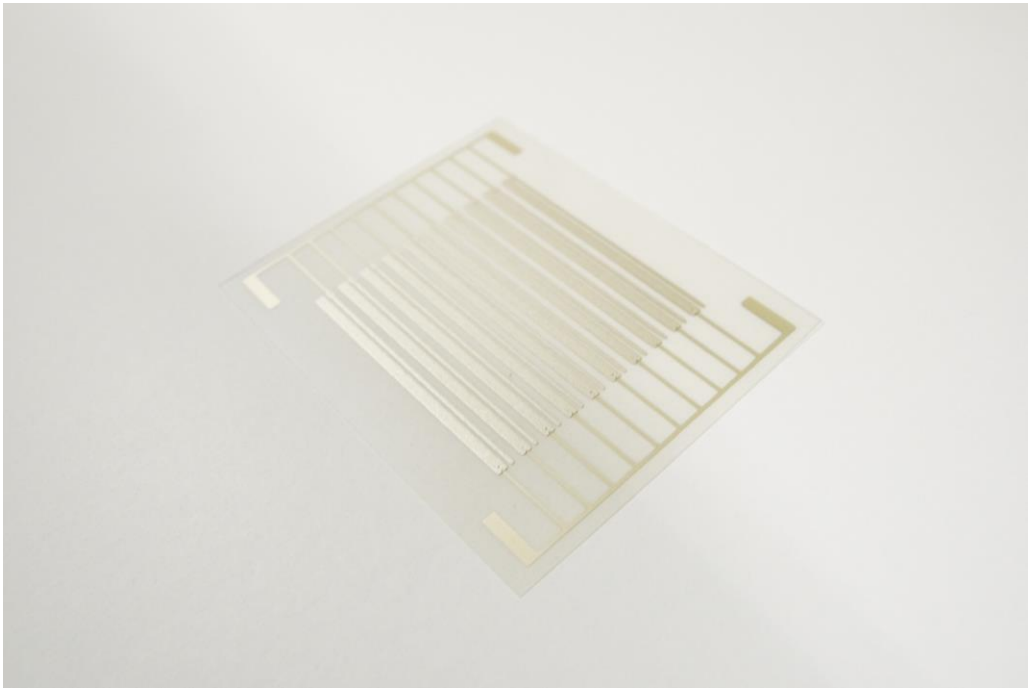

Nozzle pump

Radial pump

APPENDIX E: Supports for Pumps Designs

Macro-scale pump in a thin film configuration

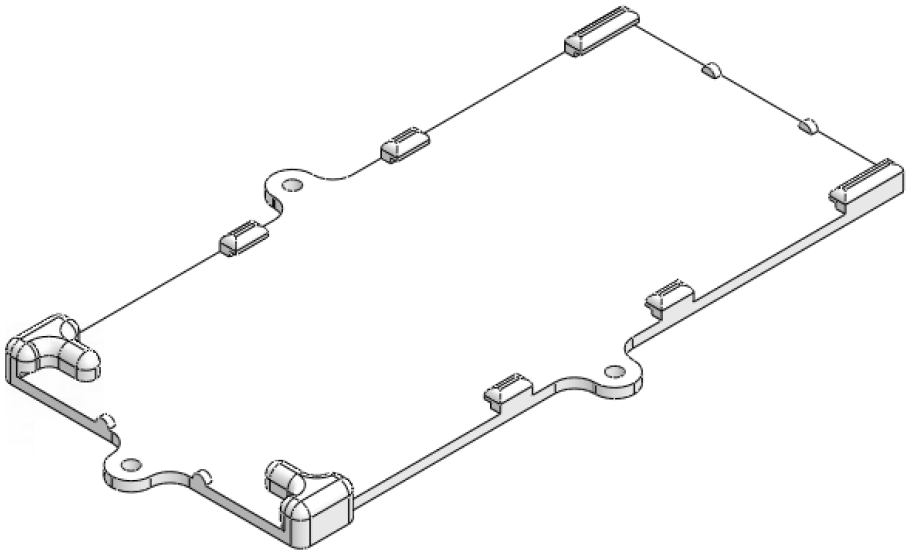

Macro-scale pump in a half cylinder configuration

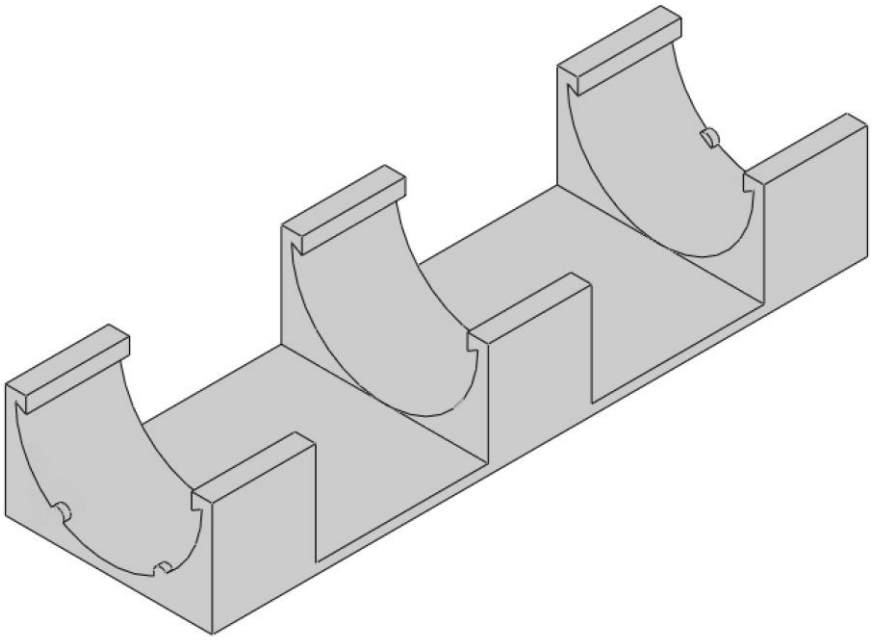

Meso-scale pump in a thin film configuration

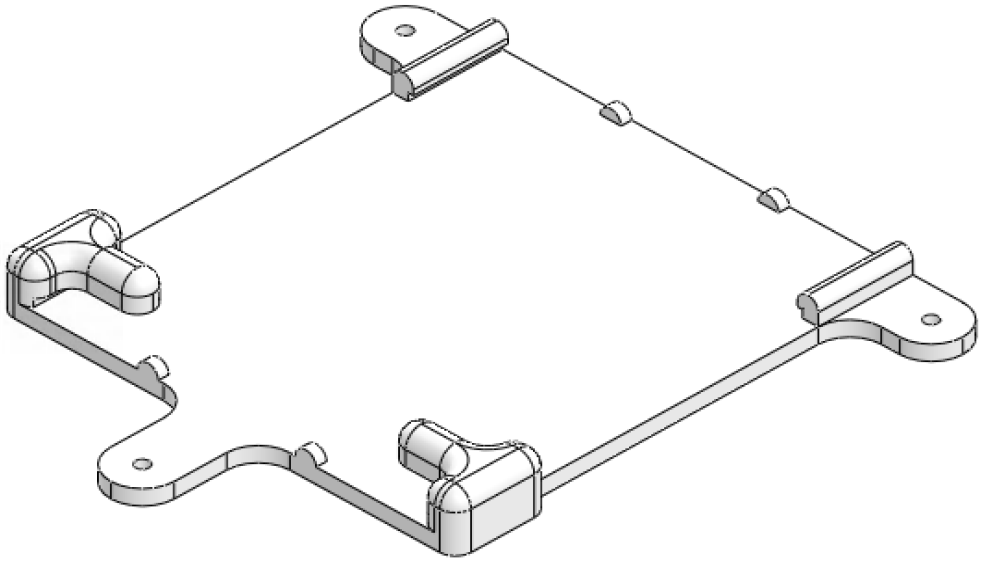

Radial pump in thin film configuration

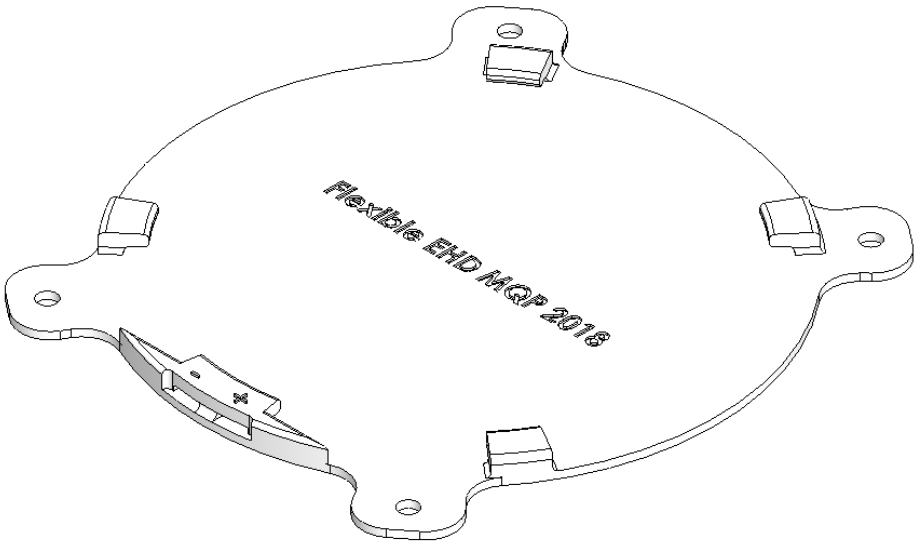

Macro-scale pump in cylinder configuration

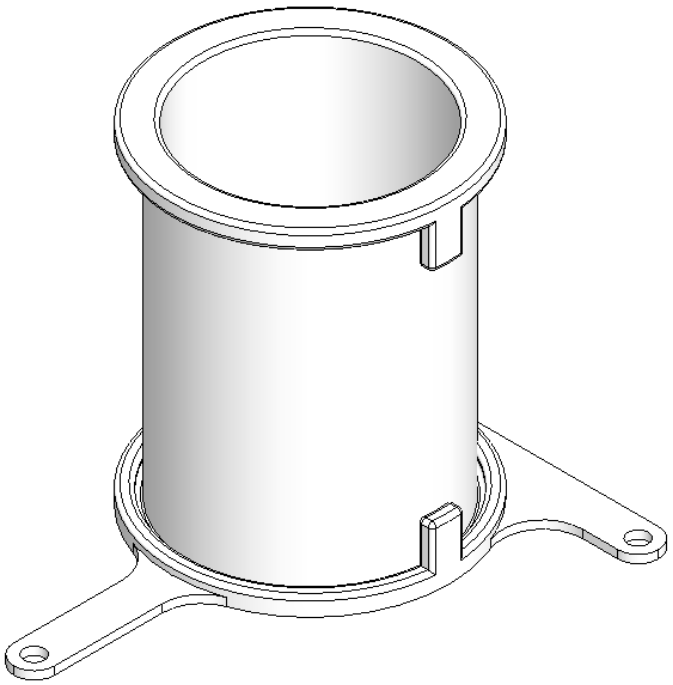

Nozzle pump in thin film configuration

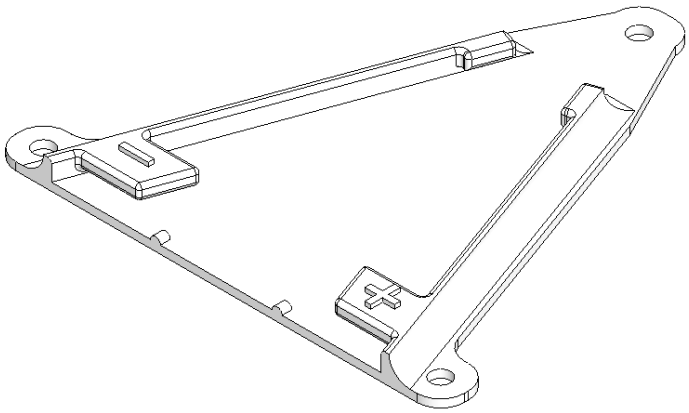

Nozzle pump in nozzle configuration

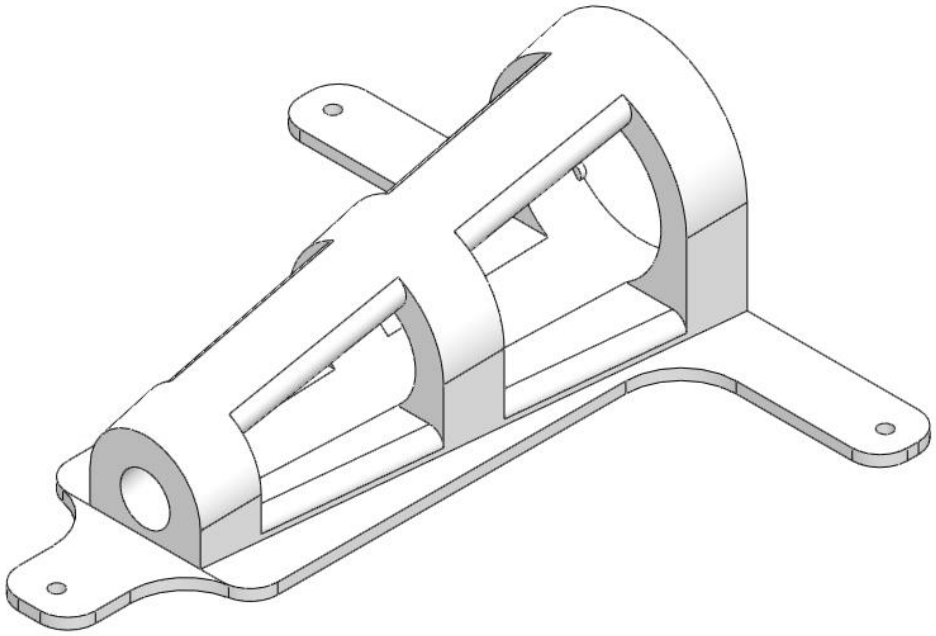

APPENDIX F: Poster for Final Presentation

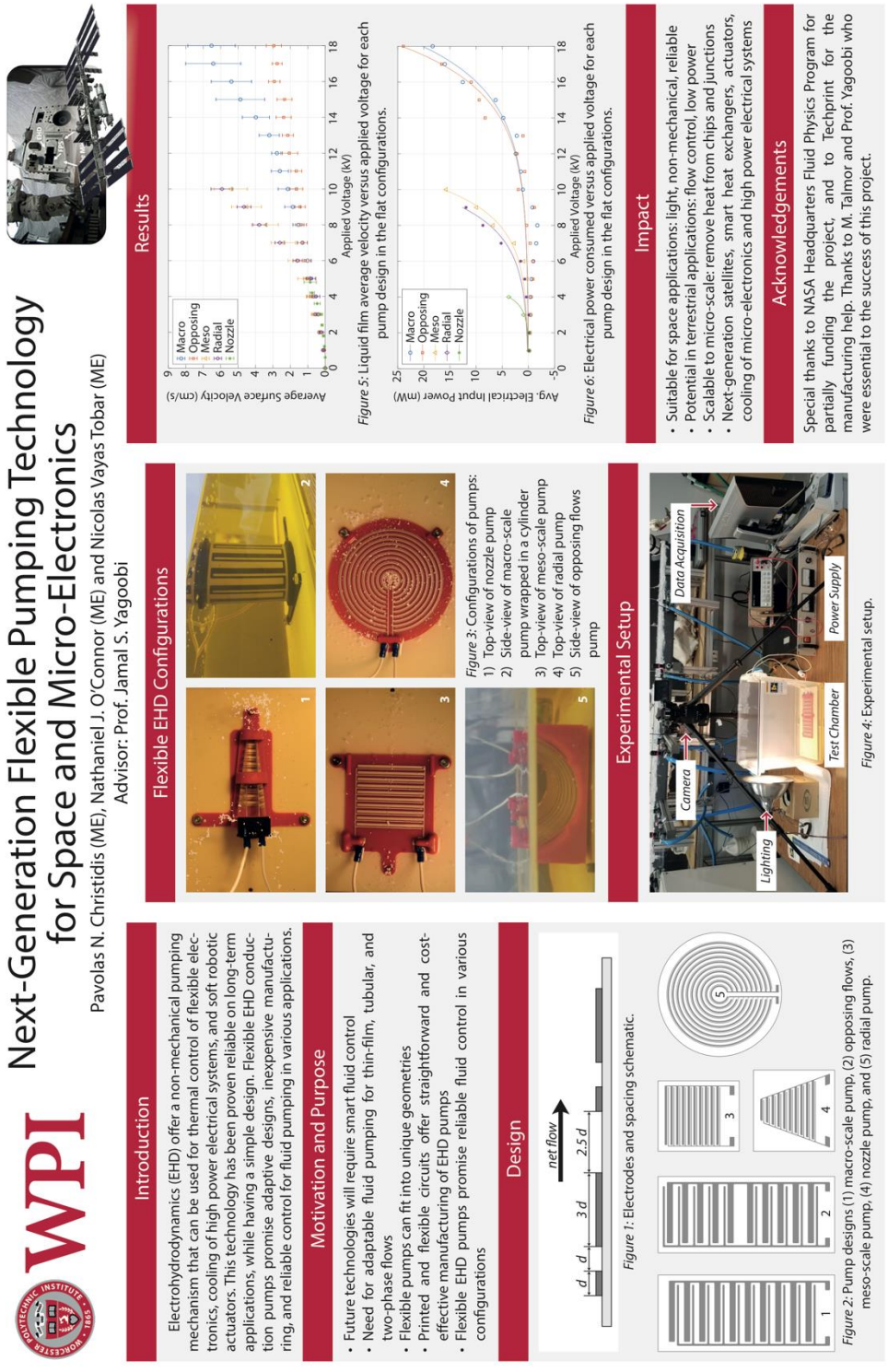

APPENDIX G: Techprint Final Prototype Drawing Order

APPENDIX H: Velocity Plot Code

MATLAB code to plot average velocity against voltage with error bars

```
% Graph results for Macro, Mixing, Meso, Circular pumps
clc; clear; close all;

file_read = 'ResultsFinal1.xlsx';

MacroData = xlsread(file_read,'Macro');
MixData = xlsread(file_read,'Mixing');
MesoData = xlsread(file_read,'Meso');
CirData = xlsread(file_read,'Circular');
NozzData = xlsread(file_read,'Nozzle');

MacroData = [0,0,0;MacroData];
MixData = [0,0,0;MixData];
MesoData = [0,0,0;MesoData];
CirData = [0,0,0;CirData];
NozzData = [0,0,0;NozzData];

hold on
errorbar(MacroData(:,3),MacroData(:,1),MacroData(:,2),'o')            %,MixData(:,1),MixData(:,2),'-
s',MesoData(:,1),MesoData(:,2),'-^',CirData(:,1),CirData(:,2),'-d')
errorbar(MixData(:,3),MixData(:,1),MixData(:,2),'s')
errorbar(MesoData(:,3),MesoData(:,1),MesoData(:,2),'^')
errorbar(NozzData(:,3),NozzData(:,1),NozzData(:,2),'d')
errorbar(CirData(:,3),CirData(:,1),CirData(:,2),'*')

grid on

%title('Average Surface Velocity with respect to Applied Voltage on the Pumps','FontSize',15)
xlabel('Applied Voltage (kV)','FontSize',17)
ylabel('Average Surface Velocity (cm/s)','FontSize',17)
legend({'Macro          (1)','Opposing          (2)','Meso          (3)','Radial          (4)','Nozzle
(5)'},'FontSize',15,'Location','northwest')
set(gca,'fontsize',14)
%set(gcf,'units','points','position',[40,40,750,350])

%                           loglog(MacroData(:,1),MacroData(:,2),'-o',MixData(:,1),MixData(:,2),'-
s',MesoData(:,1),MesoData(:,2),'-^',CirData(:,1),CirData(:,2),'-d')
```

APPENDIX I: Current and Power Plots Code

MATLAB code to plot current and power against voltage

```
% Plot the current/power against voltage for every method
% Graph results for Macro, Mixing, Meso, Circular pumps
clc; clear; close all;
% File which has data on each page for each pump (in colums: (1) Voltage in
% kiloVolts, (2) Currrent in microAmps, (3) power in miliWatts.
file_read = '2018-2-22_Combined_I&P_Data.xlsx';
% Pump_Num = {'MacroData', 'MixData', 'MixData', 'CirData', 'NozzleData', 'MacroTaData'};

% Import the data on each page to arrays in Workspace
MacroData = xlsread(file_read,'Macro');
MixData = xlsread(file_read,'Mixing');
MesoData = xlsread(file_read,'Meso');
CirData = xlsread(file_read,'Circular');
NozzleData = xlsread(file_read,'Nozzle');
MacroTaData = xlsread(file_read,'MacroTaco');

% Calculate the appropriate power based on each voltage (the power on the
% third column may not be acurrate from Excel
MacroData(:,3) = MacroData(:,1) .* MacroData(:,2);
MixData(:,3) = MixData(:,1) .* MixData(:,2);
MesoData(:,3) = MesoData(:,1) .* MesoData(:,2);
CirData(:,3) = CirData(:,1) .* CirData(:,2);
NozzleData(:,3) = NozzleData(:,1) .* NozzleData(:,2);
MacroTaData(:,3) = MacroTaData(:,1) .* MacroTaData(:,2);

% Get single values of voltage to the nearest 10^-1
MacroData(:,1) = round(MacroData(:,1),1);
MixData(:,1) = round(MixData(:,1),1);
MesoData(:,1) = round(MesoData(:,1),1);
CirData(:,1) = round(CirData(:,1),1);
NozzleData(:,1) = round(NozzleData(:,1),1);
MacroTaData(:,1) = round(MacroTaData(:,1),1);

% Take out all the values of voltage that are not integers
int_Macro =  (mod(MacroData(:,1),1) == 0);
int_Mix =  (mod(MixData(:,1),1) == 0);
int_Meso =  (mod(MesoData(:,1),1) == 0);
int_Cir =  (mod(CirData(:,1),1) == 0);
int_Nozzle =  (mod(NozzleData(:,1),1) == 0);
int_MacroTa =  (mod(MacroTaData(:,1),1) == 0);

MacroData = MacroData(int_Macro,:);
MixData = MixData(int_Mix,:);
MesoData = MesoData(int_Meso,:);
CirData = CirData(int_Cir,:);
NozzleData = NozzleData(int_Nozzle,:);
MacroTaData = MacroTaData(int_MacroTa,:);

data_cat = zeros(1,6);

for n = 1:6
    switch n
        case 1
            data = MacroData;
            m = max(data(:,1));
            data_fin = zeros(m,7);
            for i = 1:m
                data_sort = (data(:,1) == i);
                data_curr = data(data_sort,:);
                data_cat = [i max(data_curr(:,2:3)) min(data_curr(:,2:3)) mean(data_curr(:,2:3))];
                data_fin(i,:) = data_cat;
            end
            Final_Macro = data_fin;
        case 2
```

```
            data = MixData;
            m = max(data(:,1));
            data_fin = zeros(m,7);
            for i = 1:m
                data_sort = (data(:,1) == i);
                data_curr = data(data_sort,:);
                data_cat = [i max(data_curr(:,2:3)) min(data_curr(:,2:3)) mean(data_curr(:,2:3))];
                data_fin(i,:) = data_cat;
            end
            Final_Mix = data_fin;
        case 3
            data = MesoData;
            m = max(data(:,1));
            data_fin = zeros(m,7);
            for i = 1:m
                data_sort = (data(:,1) == i);
                data_curr = data(data_sort,:);
                if isempty(data_curr)
                    continue
                end
                data_cat = [i max(data_curr(:,2:3)) min(data_curr(:,2:3)) mean(data_curr(:,2:3))];
                data_fin(i,:) = data_cat;
            end
            Final_Meso = data_fin;
        case 4
            data = CirData;
            m = max(data(:,1));
            data_fin = zeros(m,7);
            for i = 1:m
                data_sort = (data(:,1) == i);
                data_curr = data(data_sort,:);
                data_cat = [i max(data_curr(:,2:3)) min(data_curr(:,2:3)) mean(data_curr(:,2:3))];
                data_fin(i,:) = data_cat;
            end
            Final_Cir = data_fin;
        case 5
            data = NozzleData;
            m = max(data(:,1));
            data_fin = zeros(m,7);
            for i = 1:m
                data_sort = (data(:,1) == i);
                data_curr = data(data_sort,:);
                data_cat = [i max(data_curr(:,2:3)) min(data_curr(:,2:3)) mean(data_curr(:,2:3))];
                data_fin(i,:) = data_cat;
            end
            Final_Nozzle = data_fin;
        case 6
            data = MacroTaData;
            m = max(data(:,1));
            data_fin = zeros(m,7);
            for i = 1:m
                data_sort = (data(:,1) == i);
                data_curr = data(data_sort,:);
                data_cat = [i max(data_curr(:,2:3)) min(data_curr(:,2:3)) mean(data_curr(:,2:3))];
                data_fin(i,:) = data_cat;
            end
            Final_MacroTa = data_fin;
        otherwise
            fprintf('No data.')
    end
end

Final_Meso(4,:)=[]; % Correct for zeros row in this array

Macro = [Final_Macro(:,1),abs(Final_Macro(:,2)-Final_Macro(:,6)),abs(Final_Macro(:,3)-
Final_Macro(:,7)),abs(Final_Macro(:,4)-Final_Macro(:,6)),abs(Final_Macro(:,5)-
Final_Macro(:,7)),Final_Macro(:,6),Final_Macro(:,7)];
Mix = [Final_Mix(:,1),abs(Final_Mix(:,2)-Final_Mix(:,6)),abs(Final_Mix(:,3)-
Final_Mix(:,7)),abs(Final_Mix(:,4)-Final_Mix(:,6)),abs(Final_Mix(:,5)-
Final_Mix(:,7)),Final_Mix(:,6),Final_Mix(:,7)];
Meso = [Final_Meso(:,1),abs(Final_Meso(:,2)-Final_Meso(:,6)),abs(Final_Meso(:,3)-
Final_Meso(:,7)),abs(Final_Meso(:,4)-Final_Meso(:,6)),abs(Final_Meso(:,5)-
Final_Meso(:,7)),Final_Meso(:,6),Final_Meso(:,7)];
```

```
Cir = [Final_Cir(:,1),abs(Final_Cir(:,2)-Final_Cir(:,6)),abs(Final_Cir(:,3)-
Final_Cir(:,7)),abs(Final_Cir(:,4)-Final_Cir(:,6)),abs(Final_Cir(:,5)-
Final_Cir(:,7)),Final_Cir(:,6),Final_Cir(:,7)];
Nozz = [Final_Nozzle(:,1),abs(Final_Nozzle(:,2)-Final_Nozzle(:,6)),abs(Final_Nozzle(:,3)-
Final_Nozzle(:,7)),abs(Final_Nozzle(:,4)-Final_Nozzle(:,6)),abs(Final_Nozzle(:,5)-
Final_Nozzle(:,7)),Final_Nozzle(:,6),Final_Nozzle(:,7)];
MacroT = [Final_MacroTa(:,1),abs(Final_MacroTa(:,2)-Final_MacroTa(:,6)),abs(Final_MacroTa(:,3)-
Final_MacroTa(:,7)),abs(Final_MacroTa(:,4)-Final_MacroTa(:,6)),abs(Final_MacroTa(:,5)-
Final_MacroTa(:,7)),Final_MacroTa(:,6),Final_MacroTa(:,7)];

% Find fit values for curve
% Current vs Voltage
MacV = fit(Macro(:,1),Macro(:,6),'exp1');
MixV = fit(Mix(:,1),Mix(:,6),'exp1');
MesV = fit(Meso(:,1),Meso(:,6),'exp1');
NozV = fit(Nozz(:,1),Nozz(:,6),'exp1');
CirV = fit(Cir(:,1),Cir(:,6),'exp1');

% Power vs Voltage
MacI = fit(Macro(:,1),Macro(:,7),'exp1');
MixI = fit(Mix(:,1),Mix(:,7),'exp1');
MesI = fit(Meso(:,1),Meso(:,7),'exp1');
NozI = fit(Nozz(:,1),Nozz(:,7),'exp1');
CirI = fit(Cir(:,1),Cir(:,7),'exp1');

% Plot Current vs Voltage
figure
hold on
grid on
h1 = plot(MacV,Macro(:,1),Macro(:,6),'o');
h2 = plot(MixV,Mix(:,1),Mix(:,6),'s');
h3 = plot(MesV,Meso(:,1),Meso(:,6),'^');
h4 = plot(NozV,Nozz(:,1),Nozz(:,6),'d');
h5 = plot(CirV,Cir(:,1),Cir(:,6),'*');
set([h1(1) h1(2)],'Color',[0.0000 0.4470 0.7410])
set([h2(1) h2(2)],'Color',[0.8500 0.3250 0.0980])
set([h3(1) h3(2)],'Color',[0.9290 0.6940 0.1250])
set([h4(1) h4(2)],'Color',[0.4940 0.1840 0.5560])
set([h5(1) h5(2)],'Color',[0.4660 0.6740 0.1880])
%set(get(get([h1(2) h2(2) h3(2) h4(2)
h5(2)],'Annotation'),'LegendInformation'),'IconDisplayStyle','off');

%title('Average Current with respect to Applied Voltage on the Pumps','FontSize',15)
xlabel('Applied Voltage (kV)','FontSize',17)
ylabel('Average Current (ÂµA)','FontSize',17)
legend([h1(2) h2(2) h3(2) h4(2) h5(2)],{'Macro (1)','Opposing (2)','Meso (3)','Radial (4)','Nozzle
(5)'},'FontSize',15,'Location','northwest')
set(gca,'fontsize',14)
%set(gcf,'units','points','position',[40,40,750,350])

% Plot Power vs Voltage
% figure
hold on
figure
hold on
grid on
h6 = plot(MacI,Macro(:,1),Macro(:,7),'o');
h7 = plot(MixI,Mix(:,1),Mix(:,7),'s');
h8 = plot(MesI,Meso(:,1),Meso(:,7),'^');
h9 = plot(NozI,Nozz(:,1),Nozz(:,7),'d');
h10 = plot(CirI,Cir(:,1),Cir(:,7),'*');
set([h6(1) h6(2)],'Color',[0.0000 0.4470 0.7410])
set([h7(1) h7(2)],'Color',[0.8500 0.3250 0.0980])
set([h8(1) h8(2)],'Color',[0.9290 0.6940 0.1250])
set([h9(1) h9(2)],'Color',[0.4940 0.1840 0.5560])
set([h10(1) h10(2)],'Color',[0.4660 0.6740 0.1880])
%set(get(get([h1(2) h2(2) h3(2) h4(2)
h5(2)],'Annotation'),'LegendInformation'),'IconDisplayStyle','off');

%title('Average Power with respect to Applied Voltage on the Pumps','FontSize',15)
xlabel('Applied Voltage (kV)','FontSize',17)
ylabel('Average Electrical Input Power (mW)','FontSize',17)
legend([h6(2) h7(2) h8(2) h9(2) h10(2)],{'Macro (1)','Opposing (2)','Meso (3)','Radial (4)','Nozzle
(5)'},'FontSize',15,'Location','northwest')
set(gca,'fontsize',14)
```

APPENDIX J: Bill of Materials

Company Info	Item Description	Model or Part #	Qty	Unit Price (USD)	Total Price (USD)
McMaster Carr	Clear Polyester Film 0.03" thick	8567K32	1	15.53	15.53
McMaster Carr	Buna-N Rubber Sheets	86715K629	1	7.77	7.77
McMaster Carr	Copper Tape	76555A716	1	58.12	58.12
SilvertronicLeads	Toothless AC	82R5349	1	8.45	8.45
Home Depot	64 Qt. Storage Box	14978006	1	7.97	7.97
Home Depot	Clear Polycarbonate Sheet	GE-33	2	15.98	31.96
Loctite	4203 Instant Adhesive	28026	1	31.18	31.18
McMaster Carr	High-Voltage Wire	8296K11	1	20.1	20.1
McMaster Carr	Ground Blade Plugs	8094T31	1	9.48	9.48
McMaster Carr	Straight Blade Plugs	7196K31	1	9.42	9.42
McMaster Carr	Acrylic Sheet	8505K754	1	19.29	19.29
Techprint	Custom Circuit	MX1201177-01	30	15.96 and 31.81	637.8
Techprint	Custom Circuit Phase II	MX032818-05	10	LOT	990
National Instruments	USB-6001	782604-01	1	204	204

APPENDIX K: InterPACK Conference Paper

Proceedings of the ASME 2018 International Technical Conference and Exhibition on Packaging and Integration of Electronic and Photonic Microsystems
InterPACK2018
August 28-30, 2018, San Francisco, CA, USA

IPACK2018-8322

EXPERIMENTAL STUDY OF FLEXIBLE ELECTROHYDRODYNAMIC CONDUCTION PUMPING FOR ELECTRONICS COOLING

Nicolas Vayas Tobar, Pavolas N Christidis, Nathaniel J O'Connor, Michal Talmor, Jamal Seyed-Yagoobi
Multi-Scale Heat Transfer Laboratory
Department of Mechanical Engineering
Worcester Polytechnic Institute
Worcester, MA 01609, USA

ABSTRACT

As modern day electronics develop, electronic devices become smaller, more powerful, and are expected to operate in more diverse configurations. However, the thermal control systems that help these devices maintain stable operation must advance as well to meet the demands. One such demand is the advent of flexible electronics for wearable technology, medical applications, and biology-inspired mechanisms. This paper presents the design and performance characteristics of a proof of concept for a flexible Electrohydrodynamic (EHD) pump, based on EHD conduction pumping technology in macro- and meso-scales. Unlike mechanical pumps, EHD conduction pumps have no moving parts, can be easily adjusted to the micro-scale, and have been shown to generate and control the flow of refrigerants for electronics cooling applications. However, these pumping devices have only been previously tested in rigid configurations unsuitable for use with flexible electronics. In this work, for the first time, the net flow generated by flexible EHD conduction pumps is measured on a flat-plane and in various bending configurations. In this behavioral characteristics study, the results show that the flexible EHD conduction pumps are capable of generating significant flow velocities in all size scales considered in this study, with and without bending. This study also proves the viability of screen printing as a manufacturing method for these pumps.

EHD conduction pumping technology shows potential for use in a wide range of terrestrial and space applications, including thermal control of rigid as well as flexible electronics, flow generation and control in micro-scale heat exchangers and other thermal devices, as well as cooling of high power electrical systems, soft robotic actuators, and medical devices.

INTRODUCTION

Electrohydrodynamics (EHD) is the study of the interaction between applied electric fields and fluid flow fields. This interaction can induce circulation, directed flows, and fluid mixing. EHD pumping has shown great potential due to its low power consumption, fast response, non-mechanical design with no moving parts, heat transfer enhancement capabilities, and simple geometry for various applications.

The electric body force responsible for the electrical field and flow field interaction is as follows [1]:

$$\bar{f}_{EHD} = \rho_e \bar{E} - \frac{1}{2} E^2 \nabla \varepsilon + \frac{1}{2} \nabla \left[E^2 \rho \left(\frac{\partial \varepsilon}{\partial \rho} \right)_T \right] \quad (1)$$

where E is the electric field, ρ_e is the net charge density, ε is the electric permittivity, and ρ is the mass density. The first, second, and third terms describe the Coulomb force density, the dielectrophoretic force density, and the electrostriction force density, respectively. The first term is produced when free charges are present. In isothermal single-phase fluid, the second term vanishes due to lack of permittivity gradient. Generally, the electric field is a weak function of temperature. The electrostriction force is negligible for incompressible fluids.

There are three types of EHD pumping mechanisms, and all three are based on the Coulomb force: ion-drag pumping, induction pumping, and conduction pumping. In ion-drag pumping, the non-zero charge density is generated by ion injection into the fluid by a sharp emitter electrode, via corona discharge. In induction pumping, the pumping is generated by inducing an AC traveling wave that interacts with charges that accumulate in areas of significant electrical conductivity gradient [1]. However, ion-drag pumping causes erosion of the emitter electrode and degradation of the fluid's electrical

properties, and induction pumping is complex to implement and often requires the presence of significant temperature gradients.

Conduction pumping, on the other hand, has a simple working mechanism that does not affect the fluid properties. EHD conduction uses the dissociation of electrolytic impurities present within a working dielectric fluid as a source of free charges [2]-[3]. A neutral species, AB, and its positive and negative ions, A+ and B-, constantly dissociate and recombine in the dielectric fluid.

$$AB \underset{\text{Recombination}}{\overset{\text{Dissociation}}{\rightleftharpoons}} A^{+} + B^{-}$$

When the imposed electric field exceeds a threshold, typically on the order of 1kV/cm depending on the fluid characteristics, the rate of dissociation exceeds the rate of recombination. Ion motion is caused by the Coulomb force described above and results in a non-equilibrium layer of charge in the vicinity of the electrodes, known as the heterocharge layer. The thickness of the heterocharge layer depends on the dielectric fluid properties and the applied electric field. The attraction of the heterocharges to the adjacent electrodes causes a bulk fluid motion. A schematic depicting the heterocharge layers with fluid flow direction is shown in Fig. 1 [4].

The pumping method has been preferred over the two earlier ones due to its reliable long-term operation and simple electrode design. EHD pumping has been shown to significantly increase heat transport capacity with minimal power consumption [5]. Various designs have been proposed to use EHD conduction pumping in open channel and enclosed configurations, proving to be independently successful [2]-[10].

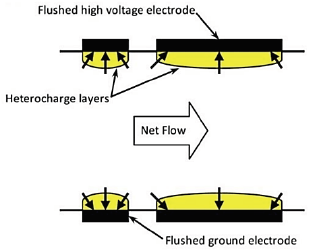

Figure 1: EHD conduction mechanism - Heterocharge layers form over electrodes, generating a net flow [4].

This paper shows the results of the first proof of concept study of flexible EHD conduction pumps, their characteristic operation in terms of generated flow velocity with and without bending, and their viability as an alternative to rigid EHD conduction pumps. The flexible EHD pumps, which consist of silver conductive ink deposited on top of a thin PET polymer film, are tested in various configurations. Each pump is bent into various shapes to prove their functionality. This research shows that these flexible pumps can be used to produce a similar flow to previous rigid EHD pumps while being manufactured in a reliable and inexpensive way.

While these initial tests were performed on macro and meso-scale pumps, this technology has the added benefit of being applied to the micro-scale. At the micro-scale, the required voltage for these pumps to operate is significantly lower [9]. Micro-scale EHD pumps would be able to significantly enhance heat transfer from electrical components such as microprocessors, using more common voltage ranges.

EXPERIMENTAL DESIGN

The flexible EHD pump prototypes were manufactured by Techprint, a local company specializing in printed electronics products. The manufacturing method used for the deposition of electrodes onto a flexible substrate was silk-screen printing. The method forces ink through a stencil on a porous material onto a substrate. Our pumps were made using a silver conductive ink that could adhere to an electronic printing polyester substrate. Both the resistivity and conductivity were similar in magnitude to those of previous materials used in EHD conduction experiments. The silver conductive ink had a resistivity of 3.81E-7 Ohm-m, and the polyester film had a resistivity of 1E17 Ohm-m.

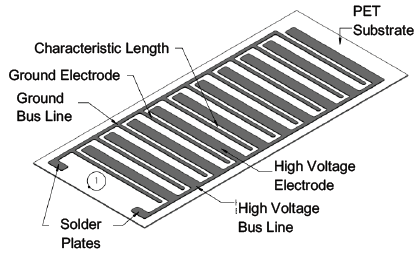

Figure 2: Macro-scale pump design (1).

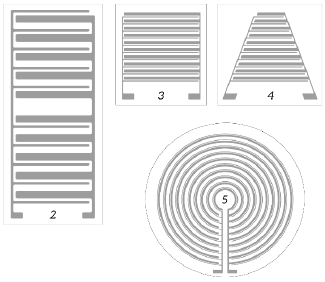

Figure 3: Additional pump designs, (2) opposing flows, (3) meso-scale pump, (4) nozzle, (5) radial.

Five different designs were printed, as shown in Fig. 2 and Fig. 3, each labeled: Straight Macro (1), Macro Opposing (2), Straight Meso (3), Nozzle (4), and Radial (5). As noted, the pumps differ in electrode configuration and size, as well as in the expected magnitude and type of flow that they will generate. The straight macro- and meso-scale pumps, as well as the radial

pumps are flexible versions of previously studied rigid pumps [11]-[12], while the opposing flow and nozzle pumps are proposed new designs for a mixing pump and converging flow accelerator, respectively. In these designs, the asymmetric electrodes results in a net Coulomb force and flow [2]. With these designs, the direction of the net Coulomb force goes from the ground electrode to the high voltage electrode. The pumps were initially tested as a flat plane pumping a thin fluid film. They were also tested as when flexed in different geometries.

From left to right, Fig. 4 shows the ground electrode, high voltage and ground electrode spacing, high voltage electrode, and electrode pair spacing. These components are also labeled in Fig. 2. The characteristic length ***d***, defined as the spacing between the high and ground voltage electrodes of an electrode pair, determines the size of each electrode and the spacing between them. The characteristic lengths are shown in Table 1, except for the radial pump. Unlike the four pumps shown in Table 1, the radial pump has a different ratio between electrodes and spacing. The radial pump has a high-voltage electrode size of 1.5*d* and an electrode pair spacing of 2.5*d*.

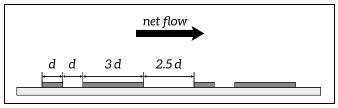

Figure 4: Electrodes and spacing schematic.

Table 1: Characteristic Dimensions for Pump Designs

	Macro Scale	Opposing Flows	Meso Scale	Nozzle
d [mm]	2.12	2.12	0.80	0.80

The characteristic length for each pump is the determining factor for how much voltage can be applied to the pump. A greater distance between the ground and high voltage electrode allows for a higher voltage to be applied. Breakdown of the working dielectric fluid occurs when the fluid medium itself begins to dissociate at the fluid's rated breakdown voltage. This results in sparking in the pump. For the macro-scale straight and opposing pumps, the maximum voltage achieved before breakdown was 18kV. For the meso-scale straight and nozzle pumps, the maximum voltage achieved before breakdown was 10kV. The radial pump, with the smallest characteristic length, was limited to 5kV before breakdown occurred.

The pumps are tested in a plastic tub container filled to a measured height with corn oil, selected because it was easy to use, less toxic than refrigerants, and cheap to obtain, while still possessing the dielectric properties required. For a proof of concept study, it was deemed to be a good option that would allow quick turnaround time between installations of each of the pump designs. The tub container material was chosen to prevent charge buildup for safety. An additional 0.625 cm acrylic slab is placed at the bottom of the tub to further insulate the pump from the tub. The tub dimensions are 35 cm by 40 cm by 60 cm. Polycarbonate glass is used to cover the top of the tub and protect measurement equipment. The power supply used in the experiment is a Glassman EH series high voltage supply capable of generating up to 30kV dc at low current. All experiments are conducted with a positive polarity for the high voltage. Blade connectors are used to connect the power supply to the electrode bus lines via the solder plates. Fixtures for the pumps were 3D printed in either ABS or PLA to hold the pumps in various geometries, simulating the insertion of the pumps into or around different configurations. The 3D printed fixtures were screwed to the acrylic slab to prevent movement of the pumps under their own pumping force. The apparatus is cleaned with isopropyl alcohol, and the corn oil is filtered through a 20μm-pore filter to prevent contamination from foreign particles. The corn oil working fluid has a dynamic viscosity of 52.3cP, dielectric breakdown of 12kV/mm, and resistivity of 1E10 Ohm-m [13]. All experiments were conducted adiabatically at room temperature (21°C - 25°C). Figure 5 shows the experimental setup and its components.

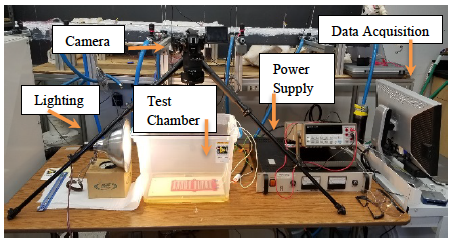

Figure 5: Experimental set-up.

A National Instrument board (USB-6001) is used for data acquisition. Applied voltage and current are monitored continuously and recorded at each voltage. The LabVIEW program controlling the experiment automatically stops the experiment from exceeding 2μA. The velocity of the liquid is measured by capturing video from a top view of the tub. 40-100μm PTFE particles were placed in the working fluid to visualize the flow. Video was captured using a Nikon D5300 camera at 60 frames per second for the entire length of the pump. The video is analyzed in Windows Movie Maker. The time taken for the particle to travel a known distance over some number of electrode pairs is recorded. Nine particles were randomly selected and analyzed at each voltage. The velocity of each particle is averaged to calculate the mean fluid velocity.

An uncertainty analysis was conducted based on the methods described by Moffat [14]. The uncertainty was calculated for each measurement voltage using the following:

$$\frac{t_{.975}\sigma_{\bar{x}}}{\sqrt{N}}$$

where $\sigma_{\bar{x}}$ is the standard deviation of the velocity at a given voltage and N is the number of samples. The error bars in the figures below represent one standard deviation from the mean velocity. For all of the pumps, the maximum uncertainty for the fluid velocity at a 95% confidence interval was 39.1%, with an average of 18.5%.

RESULTS

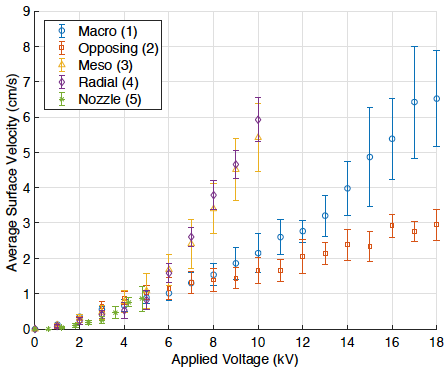

Figure 6: Liquid film average velocity versus applied voltage for each pump design.

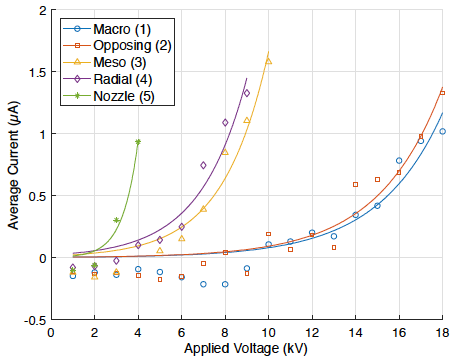

Figure 7: Current versus applied voltage for each pump design.

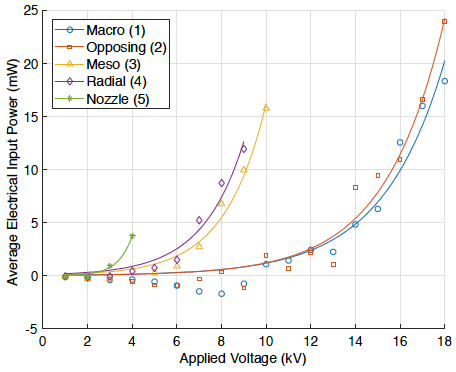

Figure 8: Electrical power consumed versus applied voltage for each pump design.

Figure 6 illustrates the change in average fluid velocity with respect to applied voltage. The error bars on the plot show one standard deviation from the average velocity. Data were taken at every 1 kV, except for the nozzle pump which has data recorded at every 0.6 kV due to the lower voltage range that could be applied to it prior to sparking. Figures 7 and 8 show the current and input power with respect to the applied voltage. The current and velocity appear to increase non-linearly with applied voltage, which is consistent with the theory and previously tested EHD conduction pumps in varying scales. While the current and power increase non-linearly, the current is only on the order of one μA and the electrical power consumption is on the order of 10mW at the high applied potential level. The same pumps are tested in different geometries but are still able to return to their original flat shape.

A. Macro-Scale Pumps

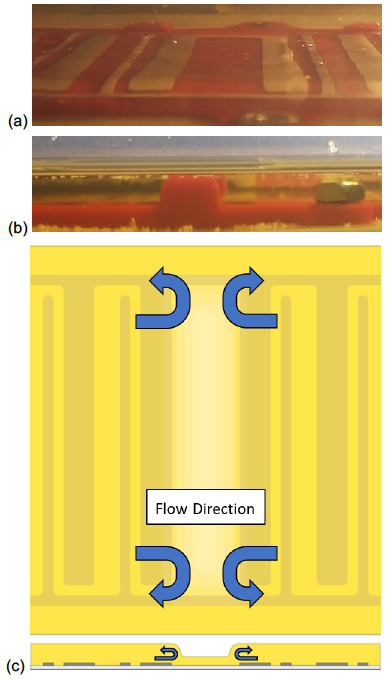

Figure 9: Mixing pump low-pressure area, (a) top view, (b) side view, (c) schematic of the flow from the top and side.

The macro-scale pump designs generated significant liquid flow at the peak of their voltage range, on the order of cm/s. This is consistent with the velocities obtained by previous studies by Siddiqui and Seyed-Yagoobi [11] on rigid EHD conduction pumps with a similar geometry, which achieved velocities between 4cm/s and 7cm/s. These pumps are tested at

a liquid film thickness of 5mm, as well as in a semi-cylindrical configuration. The unidirectional design achieved a maximum average velocity of 6.52 cm/s at an applied voltage of 18kV.

The opposing design achieved a maximum average velocity of 2.94 cm/s at 18kV. It is expected that the opposing design would have about half the average velocity or less in a given direction due to the number of electrode pairs. The number of electrode pairs linearly increases the flow rate of the pump up to a certain level. The straight macro-scale pump has ten electrode pairs in one direction, while the opposing pump has five electrode pairs in each direction. Additionally, the electrodes in the opposing pump were working against one another, further reducing the average velocity. The opposing pump had a unique characteristic: the film height was significantly reduced in the center, as shown in Figure 9. This was due to the fluid recirculated on the surface of the tub, resulting in particles appearing to move in the opposite direction of the pumping force. This is a consequence of the open container environment rather than utilizing channels to direct flow.

The presence of the bus lines on the same surface as the electrodes resulted in significant vortices on the edges of the pumps. Each bus line interacts with the opposite electrode to create a miniature electrode pair. This interaction caused recirculation through the sides of the pump.

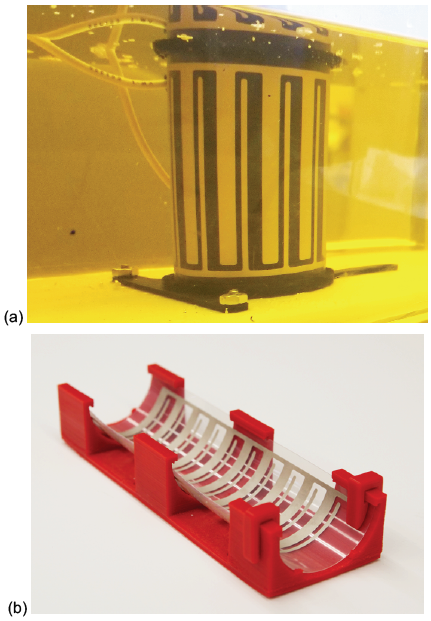

Figure 10: Macro-scale pump (a) wrapped cylindrically (b) flexed in semi-cylindrical configuration.

The macro-scale pumps in a semi-cylindrical and cylindrical geometry, both shown in Figure 10a and 10b respectively, also generated similar flow velocities at the surface of the working fluid. It is important to note that these flow velocities are measured with particles on the surface of the fluid, as the top view camera did not clearly capture any particles moving below the surface. The maximum average surface particle velocity was 4.8 cm/s at 18 kV for the macro pump. The semi-cylindrical design tended to cause a vertical circulation where fluid was pumped under the surface by the electrodes and then recirculated on the surface in the opposite direction of the pumping force. The cylindrical pump configuration was intended to create a circular flow around the tub. It was successful; however, the surface velocity was low due to the relatively small size of the pump compared to the volume of liquid in the tub container.

B. Meso-Scale Pumps

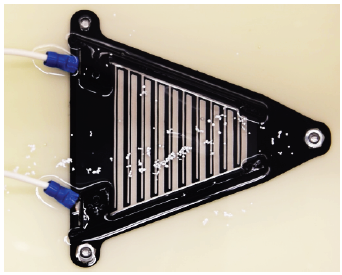

Figure 11: Nozzle pump in flat configuration.

The meso-scale pumps were tested at a liquid film thickness of 3mm and gave similar results. The maximum applied voltage for the straight meso-scale pump and nozzle pump reached 10kV compared to the radial pump, which reached 4.8kV because of the breakdown limitation of the radial pump's smaller characteristic distance. For the same reason, the radial pump was tested at smaller voltage increments. Similar to the macro-scale pumps, the unidirectional pumps achieve a higher average velocity when compared to the radial pump which has opposing flows. The straight meso-scale pump achieved a maximum average velocity of 5.42 cm/s at 10kV. The nozzle pump achieved a maximum average velocity of 5.93 cm/s at 10kV. The nozzle pump in its flat geometry had slight differences in its fixture, as shown in Figure 11, namely that the sides of the pump are contained within walls on the fixture to create the nozzle. This prevented recirculation from the sides of the pump, unlike the other pump fixtures. The walls also resulted in significant acceleration of the particles similar to a traditional nozzle due to decrease in the cross-sectional area (i.e., converging nozzle configuration). Again, similarly to the macro-scale pumps, the presence of the bus lines on the same surface of the electrodes tended to cause vortices near the edges of the pump. This was especially prevalent with the nozzle

pump as the outlet of the pump is only about 20mm wide. The vortices at the outlet of the pump slowed the particles as they exit the nozzle. Relocating the bus lines would likely improve the overall performance of this pump.

The radial pump achieved a maximum average velocity of 0.86 cm/s, which is lower compared to the other pumps. There are several reasons why the performance of this pump was apparently hindered. First, radial EHD conduction pumps such as this are typically used in a phase change type situation, where the fluid pumped into the center absorbs the heat from a source and vaporizes [15]. In the case of this experiment, no phase change is occurring, and thus a mass transport issue occurs as the fluid pumped into the center cannot easily circulate out. This results in significant resistance to the generated flow. Additionally, the PTFE particles used to measure the velocity of the fluid were on average larger than the characteristic length of the pump's electrodes. This produces unwanted interaction between the particles and the electrodes, resulting in inaccurate velocity measurements.

CONCLUSION

EHD conduction pumping was experimentally investigated in macro-, and meso-scales as a proof of concept flexible pump. The flexible conduction pumps were used in a number of configurations to drive corn oil within a contained system successfully. These flexible pumps were able to be bent and return to their original shape with no loss in performance. Flexible EHD conduction pumps were proven to have similar capabilities compared to conventional rigid EHD conduction pumps, with velocities on the same order of magnitude as their rigid counterparts. Though further work would be required to bring flexible EHD conduction pumps to the micro-scale, the concept of a flexible EHD conduction pump has been proven viable. These flexible EHD conduction pumps are the first of their kind and have significant potential.

ACKNOWLEDGEMENTS

This work was partially supported by the NASA Headquarters Fluid Physics Program.

REFERENCES

[1] Melcher, J., *Continuum Electromechanics*. Cambridge, Mass.: MIT Press (1981).

[2] Jeong, S., Seyed-Yagoobi, J., and Atten, P., "Theoretical/Numerical Study of Electrohydrodynamic Pumping through Conduction Phenomenon", *IEEE Transactions On Industry Applications*, vol. *39.2*, pp. 355-361 (2003).

[3] Atten, P., and Seyed-Yagoobi, J., "Electrohydrodynamically Induced Dielectric Liquid Flow through Pure Conduction in Point/Plane Geometry", *IEEE Transactions On Dielectrics And Electrical Insulation*, vol. *10*.1, pp. 27-36 (2003).

[4] Patel, V., & Seyed-Yagoobi, J., "Recent Experimental Advances in Electrohydrodynamic Conduction Pumping Research." *2014 IEEE Industry Application Society Annual Meeting*. pp. 1-10 (2014).

[5] Bryan, J. E. and Seyed-Yagoobi, J., "Heat Transport Enhancement of Monogroove Heat Pipe with Electrohydrodynamic Pumping" *Journal of Thermophysics and Heat Transfer*, vol. 11.3, pp. 454-460 (1997).

[6] Hanaoka, R., Nakamichi, H., Takata, S., & Fukami, T, "Distinctive Flow Properties of Liquid Jet Generated by EHD Pump and Conical Nozzle", *Electrical Engineering In Japan*, vol. *154*.1, pp. 9-19 (2005).

[7] Jeong, S., & Seyed-Yagoobi, J., "Fluid circulation in an Enclosure Generated by Electrohydrodynamic Conduction Phenomenon", *IEEE Transactions on Dielectrics and Electrical Insulation*, vol. *11*.5, pp. 899-910 (2004).

[8] Patel, V., & Seyed-Yagoobi, J.. "Dielectric Fluid Flow Generation in Meso-tubes with Micro-scale Electrohydrodynamic Conduction Pumping." *2011 IEEE International Conference on Dielectric Liquids*. pp. 1-4 (2011).

[9] Pearson, M., & Seyed-Yagoobi, J.. "Electrohydrodynamic Conduction Driven Single- and Two-Phase Flow in Microchannels with Heat Transfer." *ASME Journal of Heat Transfer*, vol. *135*, pp. 101701-101710 (2013).

[10] Louste, C., Artana, G., Moreau, E., & Touchard, G., "Sliding Discharge in Air at Atmospheric Pressure: Electrical Properties", *Journal of Electrostatics*, vol. *63*, pp. 615-620 (2005).

[11] Siddiqui, M.A. and Seyed-Yagoobi, J., "Experimental study of pumping of liquid film with electric conduction phenomenon", *IEEE Transactions on Industry Applications*, 45(1), pp.3-9 (2009).

[12] Patel, V.K. and Seyed-Yagoobi, J, "A mesoscale electrohydrodynamic-driven two-phase flow heat transport device in circular geometry and in-tube boiling heat transfer coefficient under low mass flux", *Journal of Heat Transfer*, 137(4), p.041504 (2015).

[13] Taslak, E., Kocatepe, C., Arikan, O., & Kumru, C.. "Electrical Analysis of Corn Oil as an Alternative to Mineral Oil in Power Transformers." *IJEPE*, vol. *9*.8, pp. 873-877 (2015).

[14] Moffat, R., "Describing the Uncertainties in Experimental Results". *Experimental Thermal And Fluid Science*, vol. 1, pp. 3-17 (1988).

[15] Patel, V.K. and Seyed-Yagoobi, J., "Combined Dielectrophoretic and Electrohydrodynamic Conduction Pumping for Enhancement of Liquid Film Flow Boiling", *ASME Journal of Heat Transfer*, Vol. 139, pp. 061502-1 (2017).